

Universidade de Lisboa  
Faculdade de Farmácia / Instituto Superior Técnico



**ENABLE THE DEVELOPMENT OF DISSOLUTION MODELS AS A PATH  
TO REAL-TIME RELEASE TESTING IN A CONTINUOUS  
MANUFACTURING ENVIRONMENT**

Sara Campelos Batista

Dissertation supervised by Professor António José Leitão das Neves  
Almeida and Ricardo Sousa

Masters in Pharmaceutical Engineering

2025

[Page intentionally left blank]

Universidade de Lisboa  
Faculdade de Farmácia / Instituto Superior Técnico



**ENABLE THE DEVELOPMENT OF DISSOLUTION MODELS AS A PATH  
TO REAL-TIME RELEASE TESTING IN A CONTINUOUS  
MANUFACTURING ENVIRONMENT**

Sara Campelos Batista

Dissertation supervised by Professor António José Leitão das Neves  
Almeida and Ricardo Sousa

Masters in Pharmaceutical Engineering

2025

[Page intentionally left blank]

## **Dedicatória**

Aos meus pais, por todas as oportunidades que já me proporcionaram.

À minha madrinha, por ter cumprido o papel de madrinha melhor do que ninguém.

Ao meu irmão, para que saiba que pode fazer e ser tudo aquilo que quiser.

À Rita Neves, pela empatia e altruísmo que demonstrou.

Ao Rodrigo do PAT, pela ajuda com o NIR, o Raman, e sobretudo com o SIMCA.

Ao Ricardo, por toda a paciência e pelas soluções criativas que foi arranjando.

Ao Ricardo Pereira, pela simpatia e ajuda indispensável no HPLC.

A todo o pessoal do laboratório do ODPD, pela atitude sempre bem-disposta.

Ao Telmo, por todo o amor que me demonstra todos os dias e por tudo o que já fez por mim.

I hereby declare that I have developed and written this work in strict accordance with the University of Lisbon's Code of Conduct and Good Practices. In particular, I declare that I have not engaged in any of the varieties of academic fraud which I hereby declare I am aware of, and I have followed the required referencing of phrases, extracts, images and other forms of intellectual work, fully assuming the responsibilities of authorship.

## Resumo

Num contexto de produção contínua, garantir a qualidade e conformidade do produto requer estratégias de monitorização e controlo em tempo real. O teste de dissolução, tradicionalmente realizado *offline*, continua a ser um processo demorado e que consome recursos. Este trabalho foca-se no desenvolvimento de modelos de dissolução de forma a viabilizar o *real-time release testing*, um passo crítico para aumentar a eficiência, reduzir custos e facilitar os requisitos regulatórios.

Neste trabalho, modelos mecanísticos de dissolução foram combinados com técnicas quimiométricas para permitir a previsão de perfis de dissolução de comprimidos de libertação imediata. Três modelos – *erosion*, *z-factor*, e *modified N-W* – foram avaliados nesta dissertação. As equações foram ajustadas a dados de dissolução experimentais com o objetivo de obter parâmetros otimizados. Foram construídos modelos de PLS para correlacionar os dados espectrais de misturas e comprimidos com os parâmetros das equações. Foi também realizada uma validação externa para avaliar a performance de cada modelo.

Os resultados mostraram que todos os modelos apresentaram um bom ajuste aos dados experimentais, enquanto o modelo *erosion* demonstrou o maior poder preditivo.

Adicionalmente, nesta tese foi definido um procedimento para calibrar modelos preliminares de dissolução com apenas experiências laboratoriais.

**Palavras-chave:** real-time release testing, dissolution, continuous manufacturing, model

## Abstract

In the context of continuous manufacturing, ensuring product quality and compliance requires real-time monitoring and control strategies. This work focuses on enabling the development of dissolution models as a pathway to real-time release testing, a critical step to enhance efficiency, reduce costs, and meet regulatory requirements. Dissolution testing, traditionally performed offline, remains a time-consuming and labor-intensive process.

Herein, mechanistic dissolution models were combined with chemometric techniques to allow the prediction of drug release profiles. Three models – *z-factor*, *erosion*, and *modified N-W* – were evaluated in this thesis. The equations were fitted to experimental dissolution data with the aim of obtaining optimized parameters. PLS models were built to correlate spectral data of blends and tablets to the equation parameters. External validation was also performed.

Results showed that all models provide a good fitting, while the erosion model showed the highest predictive power.

Additionally, a methodology to calibrate preliminary dissolution models using only laboratory experiments was developed in this thesis.

**Keywords:** real-time release testing, dissolution, continuous manufacturing, model

## Abbreviations

API – Active Pharmaceutical Ingredient

CM – Continuous Manufacturing

CMAs – Critical Material Attributes

CPPs – Critical Process Parameters

CQAs – Critical Quality Attributes

DoE – Design of Experiments

FDA – Food & Drug Administration

HPLC – High Performance Liquid Chromatography

ICH – International Council for Harmonization

MVAC – Model Validation Acceptance Criteria

NIR – Near-infrared

PAT – Process Analytical Technology

PLS – Partial Least Squares

QbD – Quality by Design

R&D – Research and Development

RMSE – Root Mean Square Error

RTRT – Real Time Release Testing

RTRT-D – Real Time Release Testing for Dissolution

TPP – Target Product Profile

# Table of Contents

1.1	Continuous Manufacturing and RTRT.....	1
1.2	Predictive Modeling .....	2
1.3	Overview of Dissolution Models.....	4
1.4	Aim of the Study .....	8
2	Materials and Methods .....	9
2.1	Materials.....	9
2.2	DoE and Preparation of Blends .....	9
2.3	Tableting.....	10
2.4	Spectroscopy (NIR and Raman) .....	10
2.5	In-vitro dissolution testing .....	11
2.6	High-Performance Liquid Chromatography (HPLC) .....	11
2.7	Dissolution Models .....	11
2.8	Data Analysis .....	13
2.9	Tablet Disintegration Tests .....	13
3	Results and Discussion .....	15
3.1	Dissolution Profiles .....	15
3.2	Curve-Fitting.....	16
3.3	Multivariate Data Analysis and PLS Models.....	23
3.3.1	z-Factor Model.....	24
3.3.2	Erosion Model.....	28
3.3.3	Modified N-W Model .....	30
3.3.4	Assay Prediction .....	31
3.4	Overview of Model Performance.....	32
3.5	External Validation.....	34
4	Final Considerations.....	38
5	Conclusions.....	39
	References.....	40
	Annexes.....	43

## Figure Index

Figure 1 - Schematic representation of batch and continuous processes.....	1
Figure 2 - Simplified workflow for the development of the dissolution models in this work. .....	8
Figure 3 – 3-Level Full Factorial Design of Experiments (DoE). ....	10
Figure 4 - Dissolution profiles of tablets from batches B1-B8. ....	15
Figure 5 (a, b) - Dissolution profiles of batch B1 modeled by the z-factor equation and curve-fitted to the original experimental data. ....	16
Figure 6 (a-p) - Dissolution profiles of batches B1-B8, with both SF levels, modeled with the z-factor equation. ....	18
Figure 7 (a-p) - Dissolution profiles of batches B1-B8, with both SF levels, modeled with the erosion equation.....	20
Figure 8 (a-p) - Dissolution profiles of batches B1-B8, with both SF levels, modeled with the modified N-W equation.....	23
Figure 9 - Fraction of API in the tablet (blue), undissolved in solution (orange), and dissolved (dark green). ....	23
Figure 10 - Score plot for the z-factor blends model. (a) Colored according to API content. Green: 40% API. Red: 50% API. (b) Colored according to lubricant content. Green: 0.5% lubricant. Red: 1.5% lubricant. ....	25
Figure 11 - Observed vs. Predicted regression line for the z-factor blends model. ....	26
Figure 12 - Score plot for the z-factor tablet model. (a) Colored according to API content. Green: 40% API. Red: 50% API. (b) Colored according to SF level. Green: 0.75. Red: 0.85. ....	27
Figure 13 - Observed vs. Predicted regression line for the z-factor tablet model.....	28
Figure 14 - Observed vs. Predicted regression line for the erosion blends model. ....	29
Figure 15 - Observed vs. Predicted regression line for the erosion tablet model. ....	30
Figure 16 - Observed vs. Predicted regression line for the modified N-W blends model. .....	31
Figure 17 - Observed vs. Predicted regression line for the modified N-W tablets model. .....	31
Figure 18 - Observed vs. Predicted regression line for the assay models of (a) blends, and (b) tablets. ....	32
Figure 19 - External validation of the z-factor model. (a) Predicted from blend data. (b) Predicted from tablet data. Predicted dissolution profile (dark blue), confidence limits (red), experimental dissolution profile (green). ....	35
Figure 20 - External validation of the erosion model. (a) Predicted from blend data. (b) Predicted from tablet data. Predicted dissolution profile (dark blue), confidence limits (red), experimental dissolution profile (green). ....	36
Figure 21 - External validation of the modified N-W model. (a) Predicted from blend data. (b) Predicted from tablet data. Predicted dissolution profile (dark blue), confidence limits (red), experimental dissolution profile (green). ....	36

## Table Index

Table 1 - Composition of each blend in percentage (%) and respective quantities per tablet (mg).....	10
Table 2 - Equations used to model dissolution data and respective rate parameters and other inputs. ....	13
Table 3 - Calculated difference factor ( $f_1$ ) and similarity factor ( $f_2$ ) of the curve-fitted profiles. ....	33
Table 4 - Performance metrics for all the models. ....	34
Table 5 - Individual and mean rate parameters, and RMSEcv values obtained in SIMCA for blend and tablet models. ....	34
Table 6 - Assay content predicted for blend B9 and tablet B9, and respective mean values. ....	35
Table 7 - Calculated difference factor ( $f_1$ ), similarity factor ( $f_2$ ), and RMSE of the external validation.....	36

# 1. Introduction

## 1.1 Continuous Manufacturing and RTRT

Since the early 2000's, big pharma companies have been trying to modernize the sector, with encouragement from regulatory entities. This comes at a time when the industry faces several challenges – rising R&D costs to develop a compound, patent expirations, longer times to product launch, demand for quality and precision medicine, and decreasing return on investment<sup>1,2</sup>.

The introduction of the Quality by Design (QbD) approach and the FDA's PAT framework have fostered a significant investment in new technologies, process understanding and process development<sup>3,4</sup>.

Aligned with these initiatives, is the implementation of continuous manufacturing (CM). The standard for pharmaceutical companies is batch manufacturing, despite time and scale-dependent processes that lack flexibility and robustness<sup>1,5</sup>. In batch manufacturing, raw materials are charged in the beginning of the process and products are discharged all at once at the end. In continuous manufacturing, process inputs and outputs are continuously fed for as long as needed, in an integrated system of unit operations, and lot size is defined by run-time, not volume<sup>1,6</sup>. Figure 1 represents some of the typical unit operations of tablet manufacturing and highlights the amount of testing and time spent in storage, and the differences in output time of batch versus continuous manufacturing.

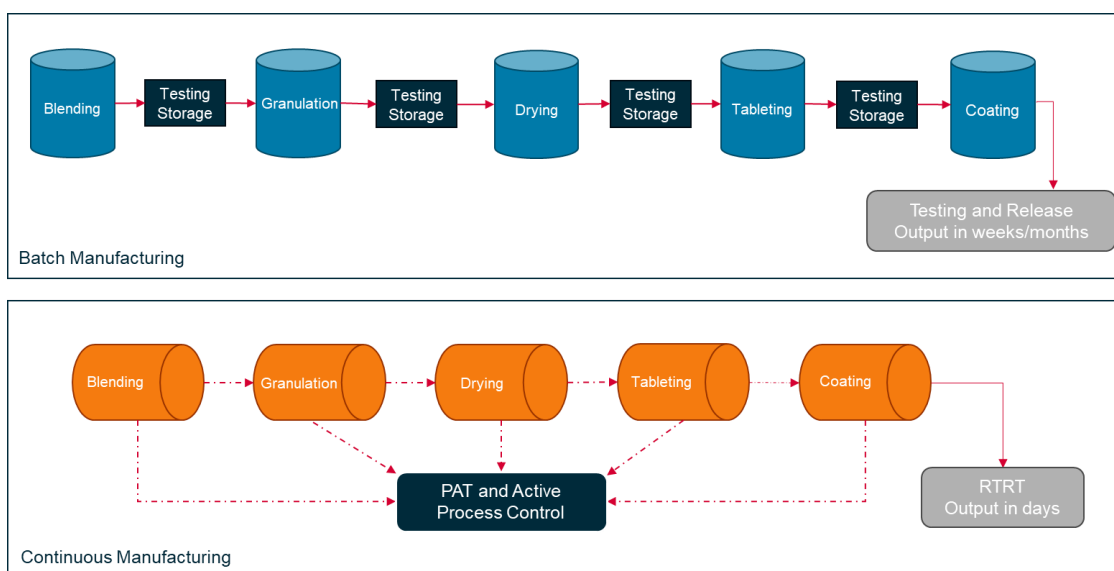


Figure 1 - Schematic representation of batch and continuous processes.

CM offers several advantages, particularly for oral solid dosage forms: batch size flexibility, easier scale up, faster response to demands, improved product quality, decreased cycle times, smaller plants with lower carbon footprints, and lower developmental and manufacturing costs<sup>1,7</sup>. Schaber et al<sup>8</sup>. published an economic analysis comparing batch and continuous processes and found that overall savings of 9 to 40% could be achieved.

As per QbD principles, quality should be inherently built into the product. This is achieved with enhanced product knowledge and process understanding<sup>5</sup>. A manufacturing process may be considered well understood when it is designed to meet product critical quality attributes consistently, and sources of process variation are identified, detected, controlled and monitored to ensure quality<sup>9</sup>.

Thus, CM benefits from the application of advanced monitoring tools, such as process analytical technology (PAT), that provide real-time measurements of material attributes and critical quality attributes (CQAs). In turn, the acquired data enables an active process control, in which critical process parameters (CPPs) are adjusted according to what the process requires to maintain desired CQAs. Ultimately, this state-of-control achieved by CM leads to improved product quality assurance and enables real-time release testing (RTRT)<sup>5</sup>.

Medicinal products must comply with approved specifications before release onto the market. Compliance with these specifications is typically evaluated by performing a set of tests on the finished product<sup>10</sup>. However, given ICH's Q8 guideline, if all necessary conditions are met, a different testing approach can be used<sup>11</sup>.

Real-time release testing is the ability to evaluate and ensure the quality of a final drug substance/drug product based on in-process data<sup>12</sup>. This strategy aims to leverage process and product understanding to reduce time and resource consuming end-product testing. It can be applied to all or certain CQAs only. In the case of the latter, a combination of conventional tests and RTRT is then used<sup>10,12</sup>.

It is worth noting that RTRT is independent of the mode of manufacture. However, citing the FDA, "it is important to recognize that the synergy of RTRT and CM affords the greatest advantages to the pharmaceutical industry when striving towards operational and regulatory flexibility"<sup>13</sup>.

## **1.2 Predictive Modeling**

Development of real-time tests includes<sup>14</sup>:

- Direct measurement of the CQA during manufacturing
- Prediction of a CQA/variable based on an empirical model

- Prediction of a CQA/variable based on a first-principles model
- Operation of CPPs within a pre-specified design space

Direct measurement of a variable/CQA is often not possible, and a discussion about design space determination is out of scope for this work. Therefore, the focus will be on the development of predictive models.

A model is a simplified representation of a system using mathematical terms. Models can enhance scientific understanding and possibly predict the behavior of a system under a set of conditions<sup>12</sup>.

The use of these models in the pharmaceutical industry was introduced along with the QbD framework and they can be applied at all stages of development or during commercial manufacturing. The overall steps to develop and implement a model are<sup>12</sup>:

- Define the purpose of the model
- Decide the modeling approach (mechanistic, empirical, etc) and possible sampling methodology
- Select variables for the model based on risk assessment, underlying physical-chemical phenomena, and process knowledge and prior experience
- Understand the limitations of the model
- Collect experimental data to support model development. Data can be collected at laboratory, pilot, or commercial scale. Variable ranges evaluated should be representative of conditions that would be expected during operation
- Develop model equations and estimate parameters
- Validate the model
- Document the outcomes of model development and create plans for verification and updating of the model throughout the lifecycle of the product.

For regulatory submissions, models can be classified into three different categories, depending on their contribution to assuring the quality of the product: low-impact, medium-impact, and high-impact models. Real-time release models are always considered high-impact, as their predictions are main indicators of product quality and will be used to make release decisions. Therefore, the approach described in the ICH's Working Group Points to Consider for model development, validation and maintenance is relevant<sup>12,15</sup>.

Quality attributes can be monitored with PAT tools such as near-infrared (NIR) or Raman spectroscopy, but typically a multivariate model (usually PLS) needs to be

developed to relate the measurement from the sensor to a variable of interest representing the CQA being tested. Chemometric models for blend homogeneity, content uniformity, moisture content and granule size, for instance, have been extensively described in literature<sup>5,15</sup>.

These are examples of empirical models, and they do not describe underlying physical-chemical phenomena (e.g. mass/energy balances, thermodynamics, transport phenomena, etc.) and so provide an incomplete process and product understanding. They also require larger calibration datasets and have a limited range of applicability in case formulation or process changes happen<sup>5,16</sup>.

As such, mechanistic (or first-principles) models derived from fundamental laws of physics, chemistry, or biology can be employed. First-principles models work with smaller datasets and extrapolate well to new conditions. Typically, developing equations that represent the system well is the main bottleneck of these models<sup>5,16</sup>.

Hybrid models that combine both mechanistic and empirical approaches to balance the advantages of each can also be used: empirical derived parameters can be inputs for first-principles models, and vice-versa<sup>16,17</sup>.

Markl et al.<sup>5</sup> provide a thorough review on RTRT for pharmaceutical tablets and include a development workflow.

### 1.3 Overview of Dissolution Models

Dissolution testing is an *in vitro* laboratory test that assesses how efficiently a drug is released from its dosage form. In manufacturing, it is used routinely as a batch release test, detecting changes in target product profiles (TPPs) or in critical quality attributes (CQAs) that might affect *in vivo* release. It is an integral part of regulatory filings for new drug applications or in demonstrating bioequivalence and approvals worldwide.

Conventional dissolution tests are destructive, lengthy and resource consuming. They require instrument calibration, sample and media preparation, and data collection (many times by HPLC). Furthermore, it is a technique prone to equipment and analyst-to-analyst variability<sup>18</sup>.

Development of a surrogate dissolution test is only possible with a mathematical model that will predict release profiles based on formulation composition, process parameters, information from spectroscopic tools, or chemical engineering first principles.

When the study of the dissolution process began, it was not related to drugs at all. In their 1897 publication, Noyes and Whitney described dissolution as a 1<sup>st</sup>-order rate process, which, when sink conditions are applied, reduces to 0-order<sup>19</sup>. According to

equation 1, the dissolution rate of a solid in a solvent is dependent on a rate parameter,  $k$  and the difference between saturation solubility,  $C_s$  and instantaneous concentration,  $C$ .

$$(1) \quad \frac{dC}{dt} = k(C_s - C)$$

Three mechanisms are responsible for dissolution of a particle: breakdown of bonds, diffusion of molecules in the boundary layer, and convection in the stirred bulk solution<sup>20</sup>. Typically, diffusion in the boundary layer is the rate-limiting step of dissolution. Later on, Nernst and Brunner related Fick's first law of diffusion to the Noyes-Whitney equation<sup>20</sup>. The equation is then represented by

$$(2) \quad \frac{dC}{dt} = -\frac{S \cdot D}{V \cdot h} (C_s - C),$$

where,  $S$  is the surface area,  $D$  is the diffusion coefficient,  $V$  is the volume of solvent, and  $h$  is the height of the boundary layer. Thus, the dissolution rate of a particle is dependent on the concentration gradient, which is in turn dependent on the diffusion coefficient, surface area, and boundary layer.  $\frac{D}{h}$  is constant during the dissolution process, while surface area changes over time.

Much work has been done on expanding the Noyes-Whitney equation and further breaking down the  $k$  constant from equation (1) into molecule and media-dependent properties. Adding dependencies and interdependencies helps identifying parameters that contribute the most to the rate constant and increases process understanding<sup>17</sup>.

Most first-principles models for predicting dissolution consist of modifications to the original Noyes-Whitney equation. The  $z$ -factor equation, described by both Nicolaidis et al. and Takano et al. is an example of that<sup>21,22</sup>.

Hofsass and Dressman<sup>23</sup> studied the suitability of the  $z$ -factor for solid dosage forms. In their publication, the relationship between initial particle mass  $M_0$  and undissolved particle mass  $M_s$  is used to describe the surface area available. Assuming all particles are spherical, with uniform particle density, initial radius  $r_0$ , and volume to surface ratio of  $\frac{r_0}{3}$ , the Noyes-Whitney equation becomes:

$$(3) \quad -\frac{dM_s(t)}{dt} = \frac{3D}{h\rho r_0} \cdot M_0^{\frac{1}{3}} \cdot M_s(t)^{\frac{2}{3}} \cdot [C_s - C(t)]$$

Since  $\frac{D}{h}$  is constant, the equation can be transformed into:

$$(4) \quad -\frac{dM_s(t)}{dt} = z \cdot M_0^{\frac{1}{3}} \cdot M_s(t)^{\frac{2}{3}} \cdot [C_s - C(t)]$$

This model assumes that at  $t=0$  the complete dose of API is immediately available for dissolution, which, as discussed by Hoffman and Dressman, can have downsides if tablets present higher disintegration times or coning happens.

Kang et.<sup>24</sup> Al also obtained fitted (predicted) dissolution curves by using a modified Noyes-Whitney model somewhat similar to the  $z$ -factor. Assuming a cylindrical tablet, and that  $S = \alpha(V_t)^{\frac{2}{3}}$ ,

$$(5) \quad \frac{dC}{dt} = k\alpha(V_t - V_d)^{\frac{2}{3}}(C_s - C_t),$$

where  $k$  is the dissolution rate constant,  $V_t$  is tablet volume,  $V_d$  is dissolved volume,  $C_s$  is solubility concentration and  $C_t$  is concentration of drug dissolved at time  $t$ . If  $k$  and  $\alpha$  are constants, and at time  $t$   $V_d$  is determined by  $C_t$ , the tablet density  $\rho$ , and solvent volume  $V_s$ , then equation (5) is converted as follows:

$$(6) \quad \frac{dC}{dt} = K(C_d - C)^{\frac{2}{3}}(C_s - C_t)$$

For more details on the transformations made to obtain this equation, the reader is directed to the original article<sup>24</sup>.

Other mathematical relationships describing dissolution based on first-principles have since appeared. For instance, Wilson et. al<sup>25</sup> used a mechanistic population balance approach to link both disintegration and dissolution in a model. To model disintegration, they assumed a cylindrical tablet with an isotropic linear erosion rate. The volume of the tablet as a function of time can then be described as:

$$(7) \quad V(t) = \frac{\pi}{4} \left( d_0 - \frac{dr}{dt} \cdot t \right)^2 \left( h_0 - \frac{dr}{dt} \cdot t \right),$$

where  $V$  is the volume of the undissolved tablet at time  $t$ ,  $d_0$  is the initial tablet diameter,  $h_0$  is the initial thickness, and  $\frac{dr}{dt}$  is the erosion rate, which is assumed constant along the dissolution.

Su et al.<sup>26</sup> also presented a population balance model for immediate-release tablets produced in a continuous extrusion-molding-coating line. To describe the change in tablet volume, an equation similar to equation (7) was used.

Regarding empirical models, much of the work has been done using near-infrared (NIR) spectroscopy in combination with multivariate data analysis<sup>27-30</sup>. Zhao et al.<sup>18</sup> predicted tablet dissolution by training PLS models with formulation, material, and process variables, NIR spectra, and a combination of both. Empirical functions - e.g. Weibull, Korsmeyer-Peppas (semi-empirical), Hixson and Crowell – can also describe dissolution profiles<sup>31</sup>. Machine learning algorithms, such as artificial neural networks, have been developed to predict dissolution profiles, with CMAs and PAT measurements as inputs.<sup>32</sup>

Examples of hybrid models have also been published. For instance, Wu et al.<sup>33</sup> combined NIR spectroscopy with mechanistic modeling to predict the dissolution behavior of film-coated modified-release tablets. In this case, empirical derived parameters were used as inputs for first-principles models.

As far as application in industry goes, a few cases have been reported. The first achieved regulatory approval of real-time release testing (RTRT) in Europe was developed by AstraZeneca and applied on a batch production line. Dissolution was predicted by a multivariate regression model, based on a design of experiments (DoE) with variations in two material attributes.<sup>34</sup>

Vertex's RTRT-D method for a CM line employs a model based on a modified Noyes-Whitney equation. The  $z$  parameter is calculated using measured material attribute results and a PLS model. Prediction of the dissolution curve's plateau is done by measuring API content in the final blend directly using in-line NIR. The predicted  $z$  and extent of release are then used to calculate the full dissolution profile. PLS models were calibrated by fitting experimental dissolution profiles to the modified Noyes-Whitney equation and determining  $z$  for each profile.<sup>34</sup>

Janssen has also developed RTRT for a batch product. Firstly, a design of experiments (DoE) is used to identify CPPs. A "process" model was built to relate CPPs to either time points on dissolution profiles or parameters of the Weibull function. A regression was then applied, with data on the content of tablets, collected by NIR, being added to the model. Finally, a predictive surrogate model based on a population average approach was developed, with inputs being CPPs and NIR content<sup>34</sup>.

Recently, the FDA has released a review of the agency's regulatory experience with RTRT for dissolution (RTRT-D)<sup>13</sup>. The aims are increasing high-quality regulatory submissions involving both CM and RTRT-D and lessening the burden of regulatory reviews. The article highlighted the most common deficiencies observed in applications

and of the thirteen case studies presented, only three were approved. Some recommendations made by the agency were as follows:

- Development of dissolution method, which should be discriminating against as many CMAs and CPPs as possible
- The real-time surrogate test should predict complete dissolution profiles, not just specific time points
- RTRT-D should be able to provide information on intra-batch variability and to reject non-equivalent drug product batches
- Sufficiently broad DoE studies that take advantage of risk assessment to identify CMAs and CPPs and their linkage to CQAs
- Justification on choice of model and thorough documentation on calibration and validation
- Justification and specification of model validation acceptance criteria (MVAC)
- Adequate sampling plan
- Plan for RTRT-D maintenance

#### 1.4 Aim of the Study

The aim of this project was to develop predictive models for dissolution with a hybrid approach. First-principles equations were fitted to experimental dissolution profiles and equation parameters were determined. PLS regressions were applied to predict the parameters from NIR and Raman spectra, and to predict the assay content of tablets. Hypothetically, these models could be applied in continuous, or batch, tableting lines for real-time release testing purposes. Methods will be further described in the next chapter, but for better understanding, a scheme of the workflow is represented in figure 2.

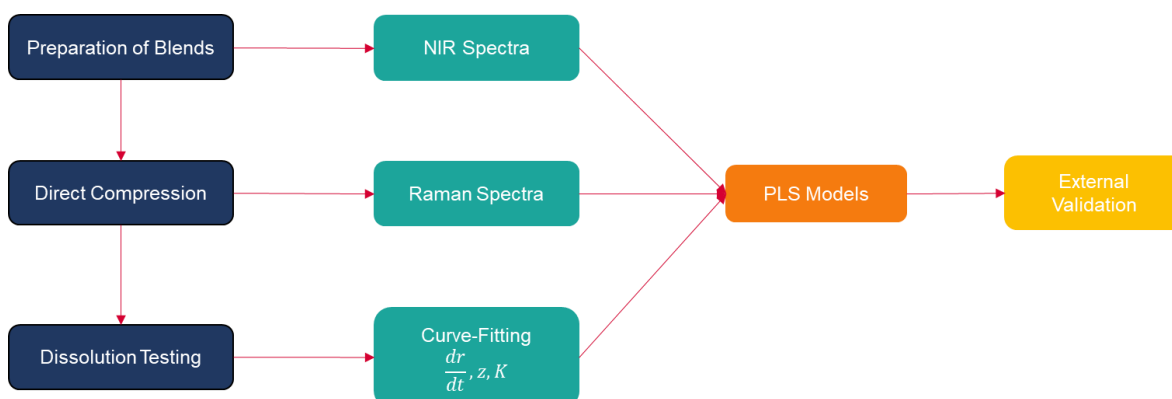


Figure 2 - Simplified workflow for the development of the dissolution models in this work.

## 2 Materials and Methods

### 2.1 Materials

For the tablets, Avicel® PH 102 microcrystalline cellulose (Hovione's material code 5510616, DuPont, DE, USA) was used as diluent, Ac-Di-Sol® sodium croscarmellose (Hovione's material code 110606, DuPont, DE, USA) as disintegrant, and magnesium stearate (Hovione's material code 110607, Merck KGaA, Darmstat, Germany) as the lubricant. The API of choice was ibuprofen (purity unknown, Hovione's material code 5512278, MolCore BioPharmatech Co., Hangzhou, PRC).

Sodium phosphate monobasic, anhydrous, purity >99% (Sigma-Aldrich, Hovione's material code 312801, MO, USA), and sodium dodecyl sulfate (Hovione's material code 5510886, Fisher Bioreagents, Loughborough, UK) were used for the dissolution medium. Formic acid, purity >98% (Hovione's material code 111452, Honeywell, NC, USA) and acetonitrile (Hovione's material code 312889, Merck KGaA, Darmstat, Germany) were used for the mobile phases. Ultrapure water was obtained from a Milli-Q® IQ 7000 water system (Merck KGaA, Darmstadt, Germany).

### 2.2 DoE and Preparation of Blends

A risk assessment was conducted to identify the material attributes and process parameters with potential impact on dissolution in a direct compression process. It was concluded that blend formulation, API attributes and tablet properties were the most interesting parameters to vary in a DoE. Unfortunately, it was not possible to obtain different API lots with varying attributes. As such, only blend formulation and tablet attributes were evaluated.

The experimental design consisted of a 3-level full factorial design (figure 3) which included three formulation variables: API, disintegrant, and lubricant percentage. A process parameter - compression force - was also varied to obtain tablets with different solid fractions. The formulation was for immediate-release, directly compressible tablets.

Thus, a total of nine blends of 25g each were prepared according to the percentages in table 1, with batch B9 acting as the center point in the DoE. Microcrystalline cellulose, croscarmellose sodium and ibuprofen were passed through a 600 µm sieve and mixed in a TURBULA® T2 GE, (WAB-Group, Muttenz, Switzerland) for 4 minutes at 32 rpm. Lubricant was also sieved, added shortly before compression and blended for another 2 min at 32 rpm.

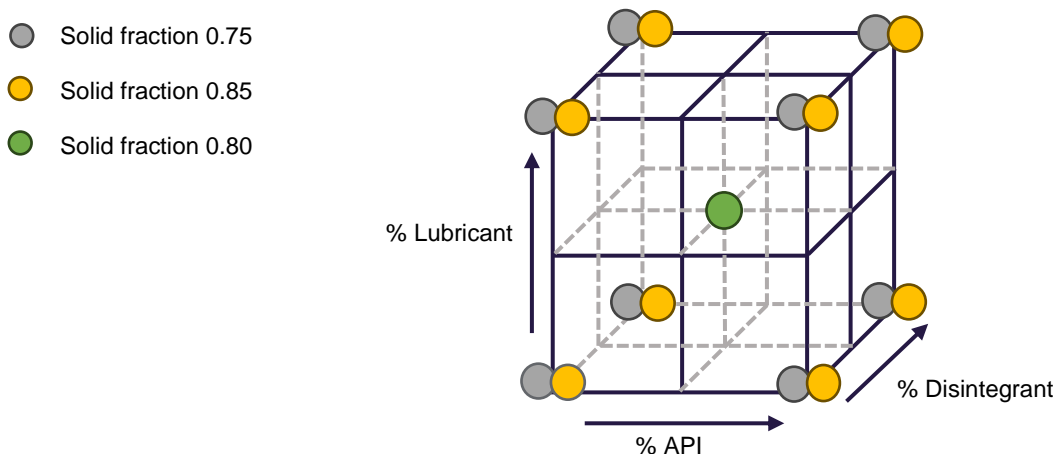


Figure 3 – 3-Level Full Factorial Design of Experiments (DoE).

Table 1 - Composition of each blend in percentage (%) and respective quantities per tablet (mg).

Batch	MCC (%)	Ac-Di-Sol (%)	Ibu (%)	MgSt (%)	MCC (mg)	Ac-Di-Sol (mg)	Ibu (mg)	MgSt (mg)
<b>B1</b>	56.5	3.00	40.0	0.50	226	12.0	160	2.00
<b>B2</b>	55.5	3.00	40.0	1.50	222	12.0	160	6.00
<b>B3</b>	51.5	7.00	40.0	1.50	206	28.0	160	6.00
<b>B4</b>	41.5	7.00	50.0	1.50	166	28.0	200	6.00
<b>B5</b>	46.5	3.00	50.0	0.50	186	12.0	200	2.00
<b>B6</b>	42.5	7.00	50.0	0.50	170	28.0	200	2.00
<b>B7</b>	45.5	3.00	50.0	1.50	182	12.0	200	6.00
<b>B8</b>	52.5	7.00	40.0	0.50	210	28.0	160	2.00
<b>B9</b>	49.0	5.00	45.0	1.00	196	20.0	180	4.00

## 2.3 Tableting

A benchtop compaction simulator (STYL'One Nano, Korsch AG, Berlin, Germany) was used to compress the powder blends into tablets. The tooling were 10 mm flat-faced, round punches and the target weight for tablets was 400 mg ( $\pm 3\%$ ). As detailed in figure 3, tablets were produced with target solid fraction (SF) values of 0.75 and 0.85 ( $\pm 0.01$ ) for batches B1-B8. For batch B9, only tablets with SF of 0.80 ( $\pm 0.01$ ) were obtained. The thickness of all tablets was measured with a digital micrometer and the density was calculated based on weight and volume.

## 2.4 Spectroscopy (NIR and Raman)

Near-infrared (NIR) spectra were collected from all blends before tableting. A probe (SentroProbe DR LS, Sentronic, Dresden, Germany) was inserted in each blend container, and reflectance values were obtained from 1100 to 2100 nm. The acquisition settings of the spectrophotometer (SentroPAT FO, Sentronic, Dresden, Germany) were

integration time of 0.01 s and an average number of 50. Three or more replicates of each blend were acquired.

Raman spectra of the tablets were collected prior to the dissolution tests. The spectrometer used was an i-Raman Prime 785S coupled with the tablet analyzer QT-Sampler (Metrohm, Herisau, Switzerland). The spectral range was 150 to 2799  $\text{cm}^{-1}$ , with laser power at 100%, exposure time of 3000 ms per scan and a total of 10 scans. Spectra were obtained of the front and back of each tablet, without replicates.

## **2.5 In-vitro dissolution testing**

A total of 17 tablets were used in the dissolution testing. Two tablets - with SF of 0.75 and 0.85 - were selected from batches B1 to B8. Additionally, a tablet with SF of 0.80 was selected from batch B9. Testing was conducted in a VK7025 Varian (Agilent, CA, USA) dissolution apparatus (USP Apparatus 2). The medium used was 50 mM phosphate buffer pH 4.5, 1% SDS. Temperature was at  $37 \pm 0.5^\circ\text{C}$ , with paddle speed at 50 rpm in 900 mL of media. A syringe with a stainless steel canula and a 35  $\mu\text{m}$  filter was used to manually draw up aliquots of 5 mL. Samples were directly placed in HPLC amber vials. Timepoints were taken at 5, 10, 20, 30, 45, and 60 min. There were no replicates ( $n=1$ ). Any samples that could not be analyzed immediately after dissolution were kept in the fridge at  $8^\circ\text{C}$ .

## **2.6 High-Performance Liquid Chromatography (HPLC)**

The samples were analyzed on an Accquity UPLC (Waters, MA, USA) to determine the amount of API dissolved at each timepoint. The method for ibuprofen analysis had already been developed prior to this work. The column used was an Accquity C18 100x2.1mm 1.7 $\mu\text{m}$  at  $35^\circ\text{C}$ . The mobile phases consisted of 0.1% formic acid in water and 0.1% formic acid in acetonitrile. Run time per sample was 25 minutes and sample temperature was kept at  $8^\circ\text{C}$ .

## **2.7 Dissolution Models**

Three models were evaluated in this thesis, and fitted to the experimental dissolution data (Excel, Microsoft Corporation, WA, USA) with the aim of obtaining optimized equation rate parameters for each tablet. The models, respective parameters, and additional inputs are described in table 1.

### **z- Factor Model**

The z-factor model was based on the integration of equation (4) assuming sink conditions ( $C_s$  at least three times higher than maximum C), which yields the equation:

$$(8) \quad M_s(t) = \left( \frac{3 \cdot M_0^{\frac{1}{3}} - M_0^{\frac{1}{3}} \cdot z \cdot t}{3} \right)^3, \text{ applicable for } t \leq \frac{3}{z}$$

The solubility saturation ( $C_s$ ) from equation (4) was removed, because it was not experimentally determined. However, this parameter is constant for all tablets since the same API was used. Therefore, it can be incorporated in the z parameter.

This model differentiates from the other models evaluated in this thesis, mostly from the assumption that all API is available for dissolution at  $t=0$ , as detailed in section 1.3 from the introduction.

### **Erosion Model**

The erosion model is based on equation (7), which describes the tablet size reduction along the dissolution time. This model assumes that the API release from the tablet is the limiting step for dissolution. This way, the API dissolved ( $M_d$ ) may be estimated from the volume reduction with the equation:

$$(9) \quad M_d(t) = [V_0 - V(t)] \cdot \rho \cdot API_{conc}$$

Where  $V_0$  is the initial volume of the tablet and  $V$  is the volume at time  $t$  estimated with equation (7).  $\rho$  is the tablet density and  $API_{conc}$  is the initial concentration of API in the formulation (weight ratio). The model parameter that dictated the dissolution rate is the erosion parameter  $\frac{dr}{dt}$  from equation (7).

### **Modified N-W Model**

The third model considered consists in a combination of equation (6) and equation (7). This model is a variation of the Noyes-Whitney equation, without the assumption that all API is available for dissolution at the beginning of the test. Instead, as disintegration proceeds, undissolved API will gradually be made available for dissolution. The API available in solution is estimated based on the volume change of the table, excluding the API that is already dissolved.

$$(10) \quad C_{API\_available}(t) = \frac{[V_0 - V(t)] \cdot \rho \cdot API_{conc}}{V_{solution}} - C(t),$$

Where the tablet volume at time  $t$  is estimated with equation (7). Equation (10) was incorporated in equation (6) resulting in the equation:

$$(11) \quad \frac{dC}{dt} = K(C_{API\_available})^{\frac{2}{3}}(C_s - C)$$

This model requires the calibration of two parameters,  $K$  and  $\frac{dr}{dt}$  to predict the dissolution profile. Table 1 summarizes the models evaluated in this work.

Table 2 - Equations used to model dissolution data and respective rate parameters and other inputs.

Model	Equation	Rate Parameter	Additional Inputs
<b>z-factor</b>	$M_s(t) = \left( \frac{3 \cdot M_0^{\frac{1}{3}} - M_0^{\frac{1}{3}} \cdot z \cdot t}{3} \right)^3$ , applicable for $t \leq \frac{3}{z}$	$z$	API Load
<b>Erosion</b>	$V(t) = \frac{\pi}{4} \left( d_0 - \frac{dr}{dt} \cdot t \right)^2 \left( h_0 - \frac{dr}{dt} \cdot t \right)$ $M_d(t) = [V_i - V_f(t)] \cdot \rho \cdot API_{conc}$	$\frac{dr}{dt}$	Tablet diameter Tablet thickness Tablet density Tablet weight API Load
<b>Modified N-W</b>	$V(t) = \frac{\pi}{4} \left( d_0 - \frac{dr}{dt} \cdot t \right)^2 \left( h_0 - \frac{dr}{dt} \cdot t \right)$ $C_{API\_available}(t) = \frac{[V_0 - V(t)] \cdot \rho \cdot API_{conc}}{V_{solution}} - C(t)$ $\frac{dC}{dt} = K(C_{API\_available})^{\frac{2}{3}}(C_s - C)$	$\frac{dr}{dt}, K$	Tablet diameter Tablet thickness Tablet density Tablet weight API Load

## 2.8 Data Analysis

PLS models for both blend and tablet datasets were developed using SIMCA (Sartorius, Göttingen, Germany) to correlate respective spectral data to the predicted model parameters. The calibration set included batches B1-B8, while batch B9 was used to perform external validation and evaluate model performance. Spectra preprocessing was also applied in SIMCA.

## 2.9 Tablet Disintegration Tests

Spare tablets with the same composition and solid fraction level as the ones dissolved were tested to provide an estimate of their disintegration time. The equipment was the SOTAX DT-50 basket-rack apparatus (SOTAX Group, Basel, Switzerland). The medium

was deionized water at  $37 \pm 0.5^{\circ}\text{C}$ . Due to tablet debris interfering with automatic end-point detection, disintegration times were recorded manually. To reduce debris buildup, only three of the six tubes were used at a time.

### 3 Results and Discussion

#### 3.1 Dissolution Profiles

Figure 4 represents the dissolution profiles obtained for the calibration set of the models - tablets from batch B1 to batch B8.

In samples with the same formulation but different SF levels, a higher SF led to slower dissolution rates. This is expected as more force was used to compress the powder. Based on the profiles obtained, it is not possible to distinguish other variations between formulations.

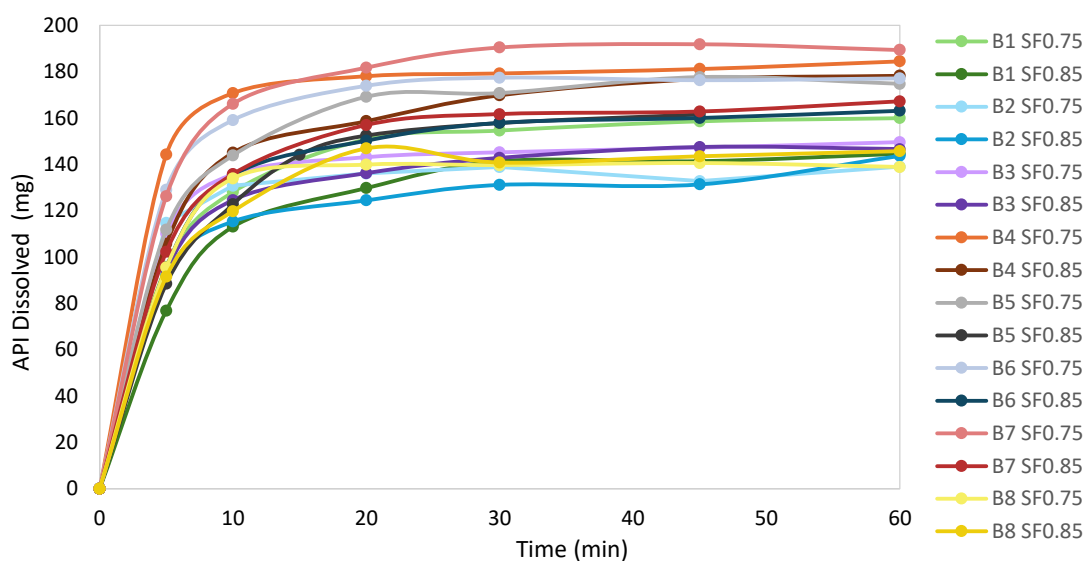


Figure 4 - Dissolution profiles of tablets from batches B1-B8.

In all experiments, the percentage of API released did not reach 100% and it is worth noting that a proper dissolution method for ibuprofen was not developed for this work due to time constraints. Firstly, the 50 mM phosphate buffer pH 7.2 (described in the USP) was tested, but complete dissolution of the API was very fast, and profiles were not discriminatory enough. Given that ibuprofen is the most soluble at pH 7.2 and its solubility decreases in lower pH levels, a 50 mM phosphate buffer pH 4.5 with 1% SDS was used instead. Solubility tests were not performed and sink conditions were not assured. Coning occurred in all experiments after dosage form disintegration. The presence of coning may affect dissolution of poorly soluble APIs, as they are not fully exposed to the medium.

Furthermore, the HPLC method used for ibuprofen quantification stated a sample temperature of 8°C. After several runs, it was realized that samples at this temperature froze and precipitated in the vials during HPLC analysis, possibly also affecting quantification. This issue, along with an inadequate dissolution medium might have

caused the incomplete dissolution of the ibuprofen and the erratic profiles obtained. As such, models might have been fitted and calibrated based on faulty data.

### 3.2 Curve-Fitting

#### z-Factor Model

The z-factor model assumes that all particles are available for dissolution, which might not have been the case since dissolution did not reach 100%. It was necessary to adjust the data according to equation (12),

$$(12) \quad API_{adj} = (API_{exp}/API_{total}) \cdot API_{load},$$

where  $API_{adj}$  is the adjusted amount of API released. The amount of drug released at each timepoint ( $API_{exp}$ ) was divided by the total API released ( $API_{total}$ ), then multiplied by the theoretical API load of the tablet ( $API_{load}$ ). This provided a normalized release profile, expressed relative to the drug content in the tablet. Had this not been done, there would have been an offset between the experimental and the modeled data. An example of the curve-fitting without adjusting the experimental data is presented in figure 5.

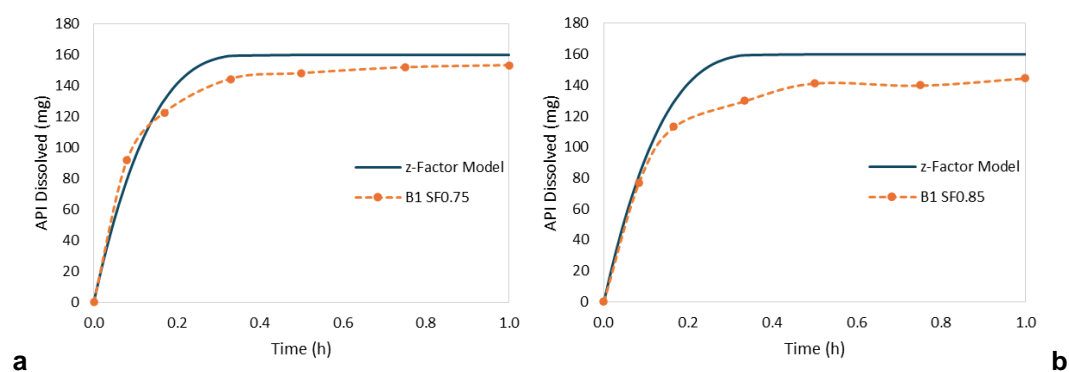
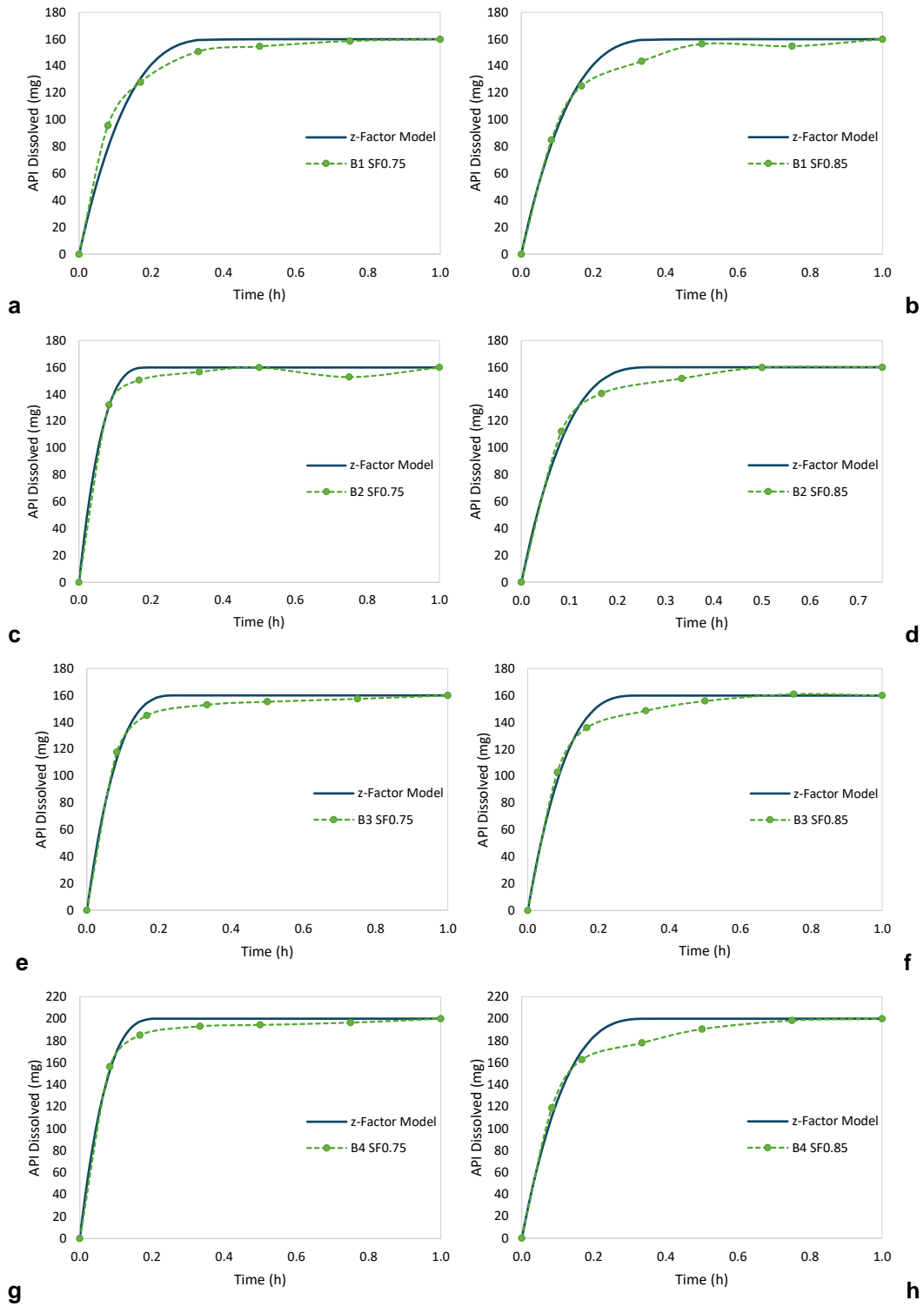


Figure 5 (a, b) - Dissolution profiles of batch B1 modeled by the z-factor equation and curve-fitted to the original experimental data.

Figure 6 (a-p) shows the modeled data with the adjusted experimental data.



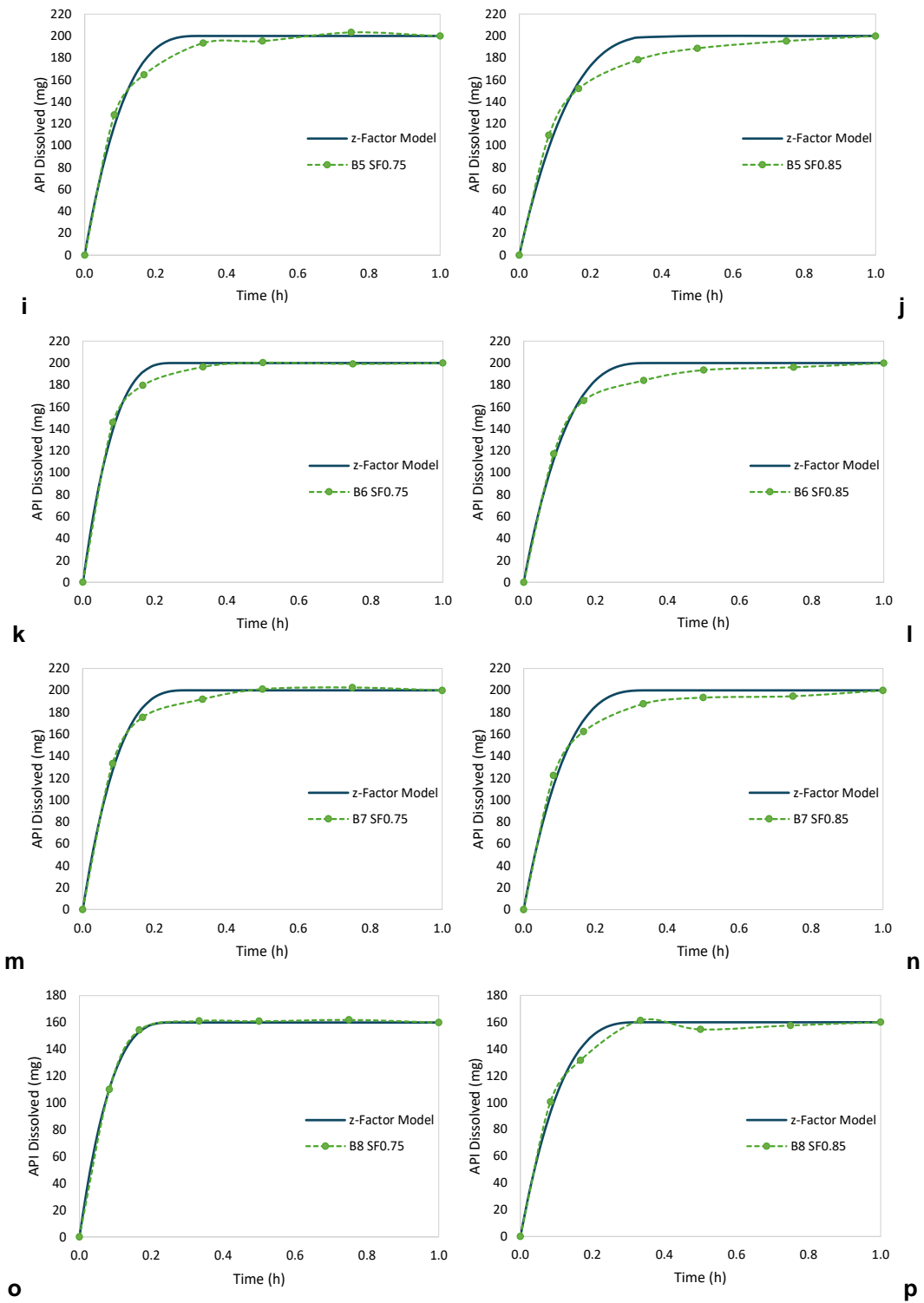
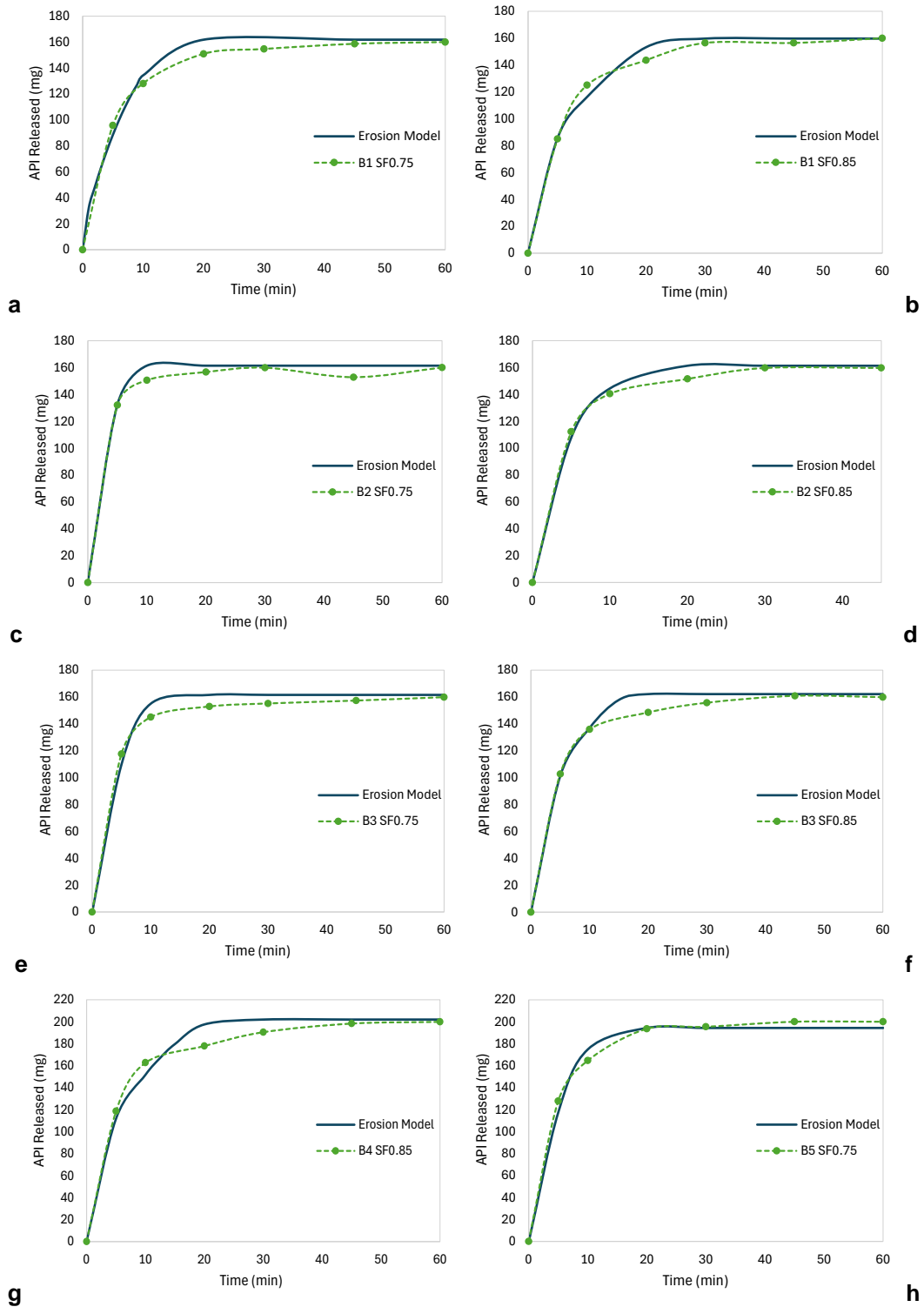


Figure 6 (a-p) - Dissolution profiles of batches B1-B8, with both SF levels, modeled with the z-factor equation.

### Erosion Model

Figure 7 (a-p) represents the dissolution curves fitted with the erosion model. The experimental drug release also needed to be adjusted according to equation (12). This model does not assume that all API is available at the beginning of the test, but instead

that the whole tablet gradually erodes, with all API being released and consequently dissolved.



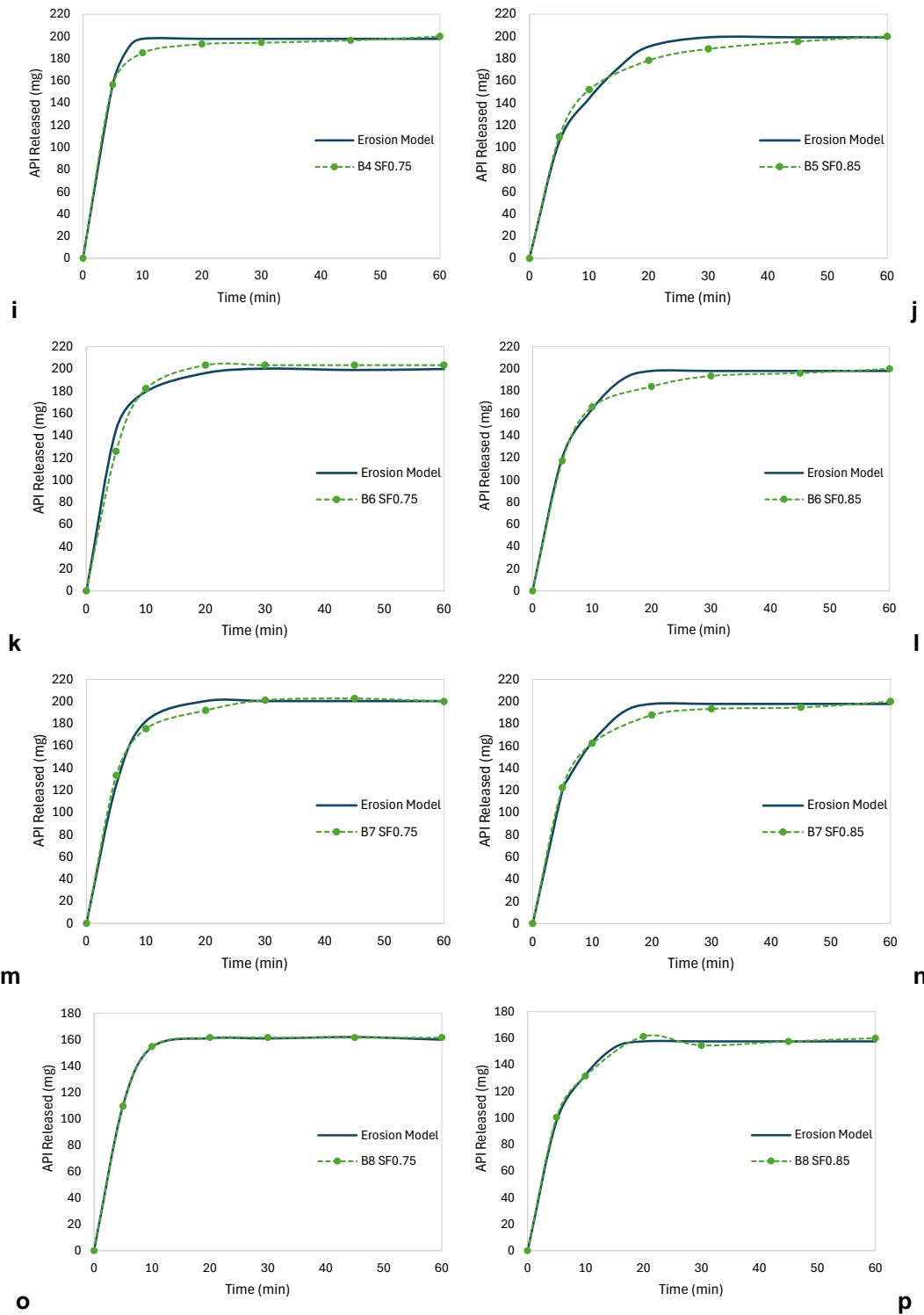


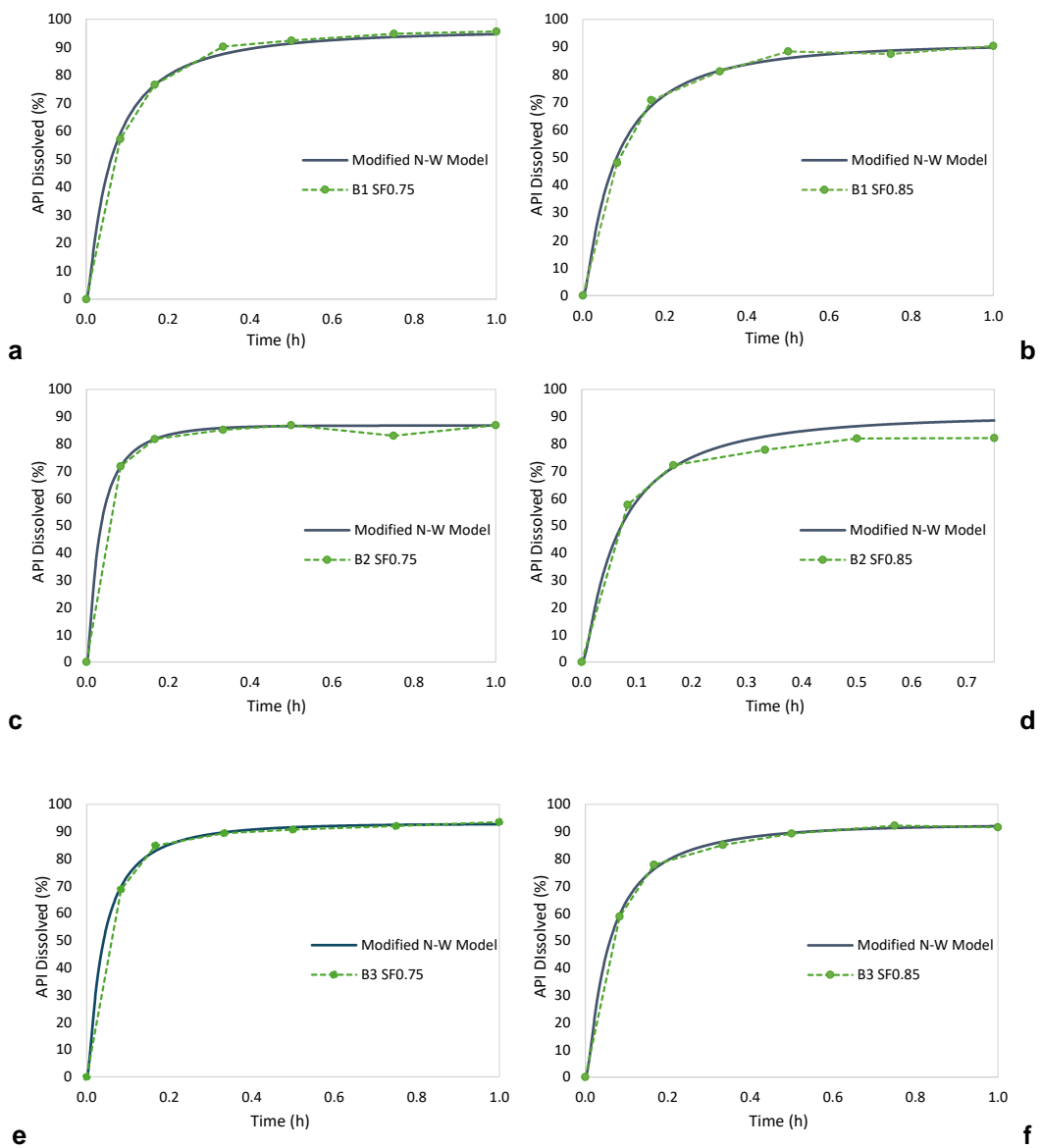
Figure 7 (a-p) - Dissolution profiles of batches B1-B8, with both SF levels, modeled with the erosion equation.

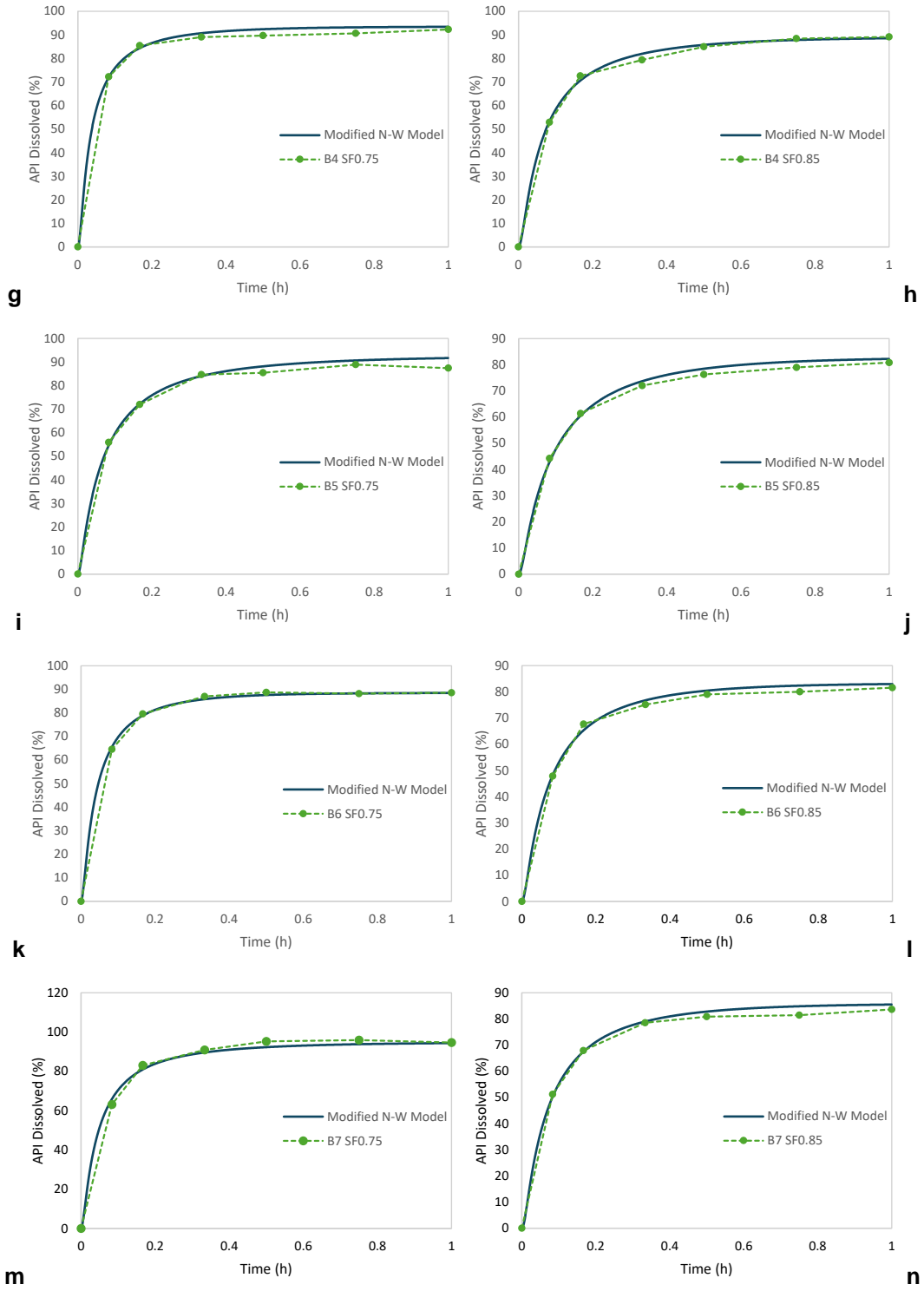
### **Modified N-W Model**

Predicted dissolution profiles obtained with the modified N-W model are presented in figure 8 (a-p). It was not necessary to adjust the experimental release as this model does not assume sink conditions. The parameter  $C_s$  was adjusted to account for the maximum solubility.

As explained previously, this equation requires the calibration of two parameters,  $\frac{dr}{dt}$  and  $\kappa$ . However, the parameter  $\frac{dr}{dt}$  was not calibrated. Instead, it was estimated based on the disintegration time of the tablets.

Disintegration tests showed that for tablets with the same SF level, the disintegration time was similar. Therefore, to calculate the  $\frac{dr}{dt}$ , the height of each tablet was divided by the mean disintegration time of either SF level. Tablets with SF of 0.75 disintegrated in approximately one minute, corresponding to a  $\frac{dr}{dt}$  of 300 mm/h. Tablets with SF of 0.85 disintegrated in about 1 min 30 seconds, which gives an erosion rate of 200 mm/h.





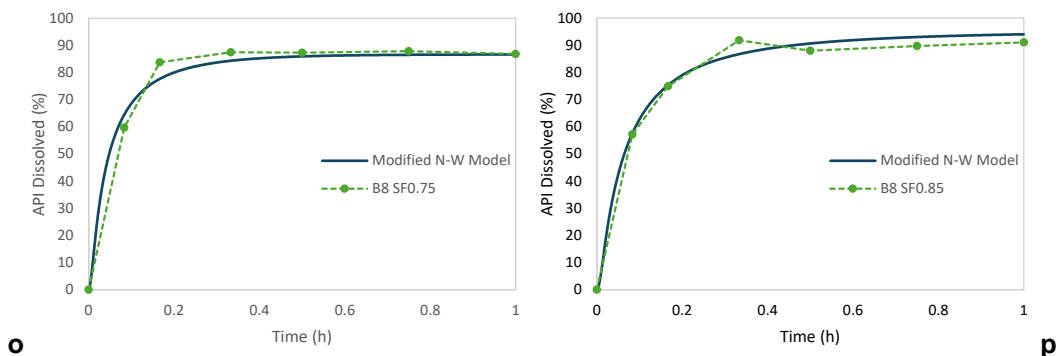


Figure 8 (a-p) - Dissolution profiles of batches B1-B8, with both SF levels, modeled with the modified N-W equation.

Figure 9 denotes the fractions of API still in the tablet, API undissolved, and API dissolved over time for tablet B1 SF0.75. The fraction of API in the tablet declines very quickly, due to rapid disintegration. As disintegration occurs and API is exposed to the medium, the fraction of undissolved API in solution increases sharply, as it becomes available to be dissolved. At one hour, it is possible to see that there is still undissolved API.

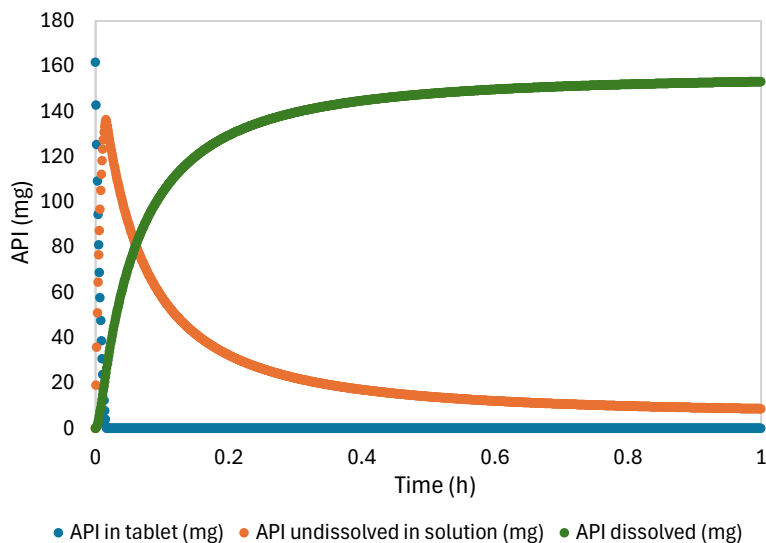


Figure 9 - Fraction of API in the tablet (blue), undissolved in solution (orange), and dissolved (dark green).

### 3.3 Multivariate Data Analysis and PLS Models

PLS models were developed to correlate blend spectra and tablet spectra to the equation parameters  $\frac{dr}{dt}$ ,  $z$ , and  $K$ . As shown in the previous section, these parameters were individually optimized for each tablet, with two tablets produced from each blend.

In order to calibrate the PLS blend models, the mean values of  $\frac{dr}{dt}$ ,  $z$ ,  $K$  were calculated for tablets with the same formulation but different solid fractions.

For the blend spectra, preprocessing involved applying a Savitzky-Golay 2nd derivative combined with standard normal variate (SNV) correction. No specific spectral region was excluded during this preprocessing. For the tablet spectra, preprocessing was performed using SNV. Additionally, the spectral region from 1640 to 2799  $\text{cm}^{-1}$  was excluded, as it was deemed to contain noise.

### 3.3.1 z-Factor Model

#### **Blends**

Figures 10a and 10b show PLS score plots from the z-factor model obtained with blend data, colored according to API (10a) and lubricant content (10b), respectively. Though there are no obvious clusters, API content influences score distribution along PC1, while PC2 separates blends with different lubricant content. The percentage of disintegrant did not seem to be explained by any component. There are no outliers apparent.

Figure 11 shows the regression line for observed versus predicted values of  $z$  for the blend data. The model was built using four components, with the following performance metrics (table 4):

$R^2X$ : 0.629

$R^2Y$ : 0.971

$Q^2$ : 0.779

The number of components for all models was chosen based on the  $R^2Y$ ,  $Q^2$  and RMSEcv (more information in annex A1). Points with the same color represent spectra replicates of each blend. It is noticeable that the replicates for blend B1 exhibit less precise predictions for the  $z$  parameter, indicating potential variability in the spectral data for this blend. This variability could have been introduced due to incorrect placement of the probe or capturing information from the plastic container, for example. To avoid this, more replicates of each blend spectra should have been acquired.

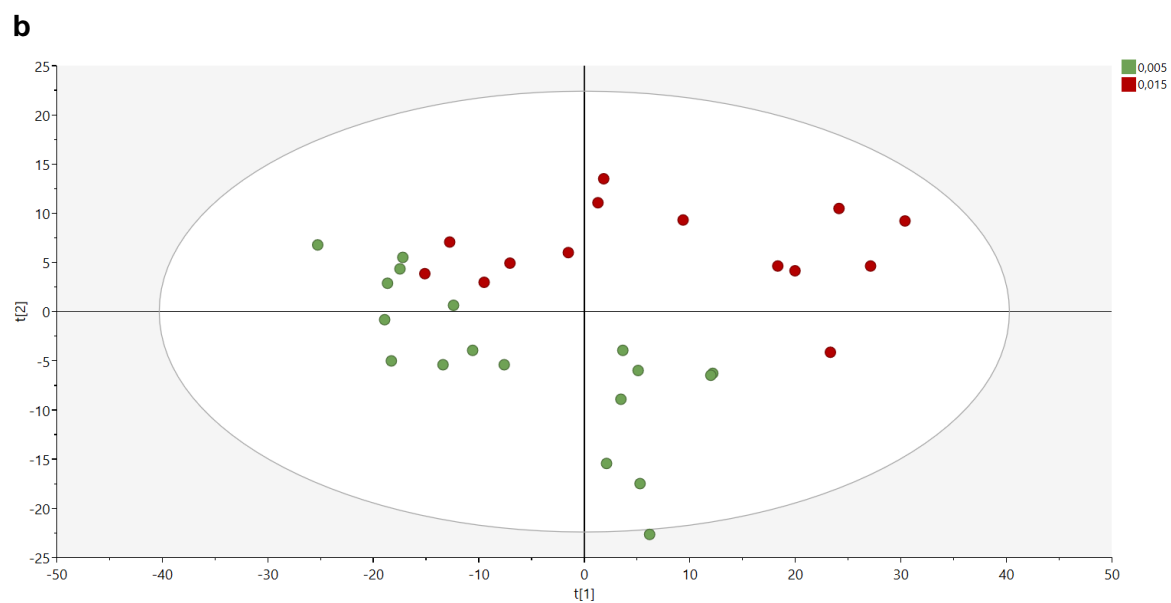
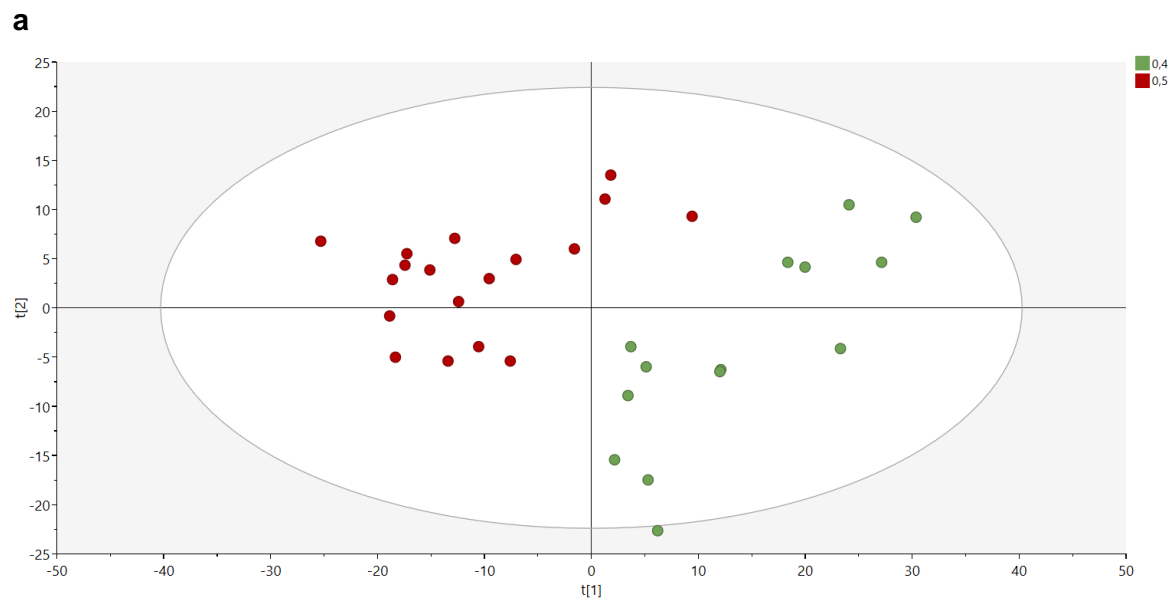


Figure 10 - Score plot for the z-factor blends model. (a) Colored according to API content. Green: 40% API. Red: 50% API. (b) Colored according to lubricant content. Green: 0.5% lubricant. Red: 1.5% lubricant.

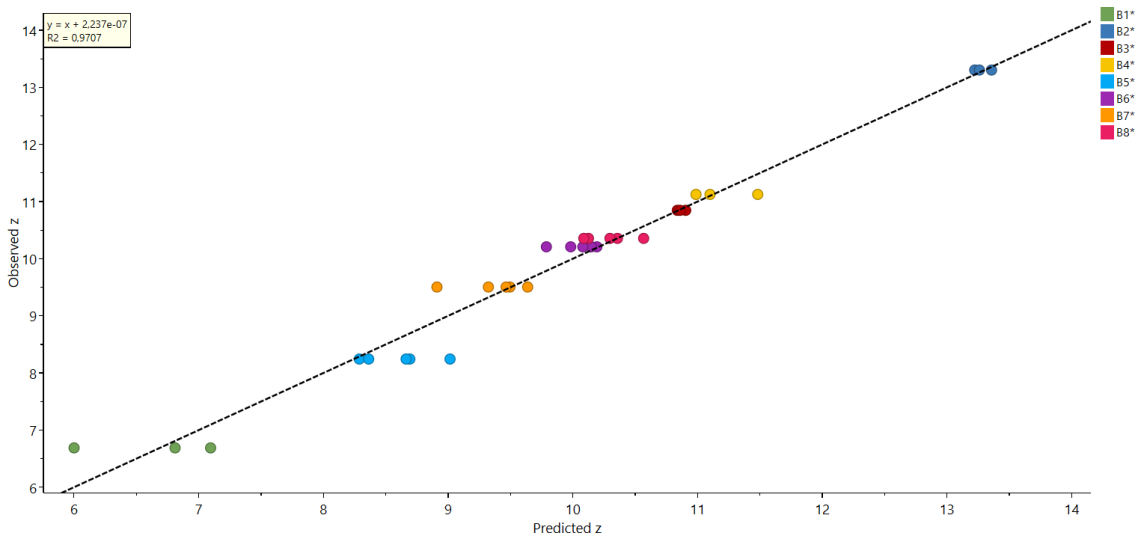


Figure 11 - Observed vs. Predicted regression line for the z-factor blends model.

## **Tablets**

Figures 12a and 12b represent the score plots also from the z-factor model but based on tablet data. Similar to the results from the blend data, disintegrant content did not show an apparent influence on the score distribution in any of the principal components. However, unlike the blend model, lubricant content did not significantly impact the score distribution in the tablet model. In the case of tablets, API content and SF level appear to be the variables most correlated to the dissolution parameters. PC2 is influenced by the API content, while SF level seems to influence the distribution both along PC1 and PC2. In all of the scores plots for tablets it is possible to identify four clusters: low API%-low SF, high API%-low SF, low API%-high SF, and high API%-high SF.

The model was built using five components, with the following performance metrics (table 4):

R<sup>2</sup>X: 0.838

R<sup>2</sup>Y: 0.989

Q<sup>2</sup>: 0.825

Figure 13 shows the regression line of observed versus predicted values of z for tablets. Data points are tightly clustered along the regression line.

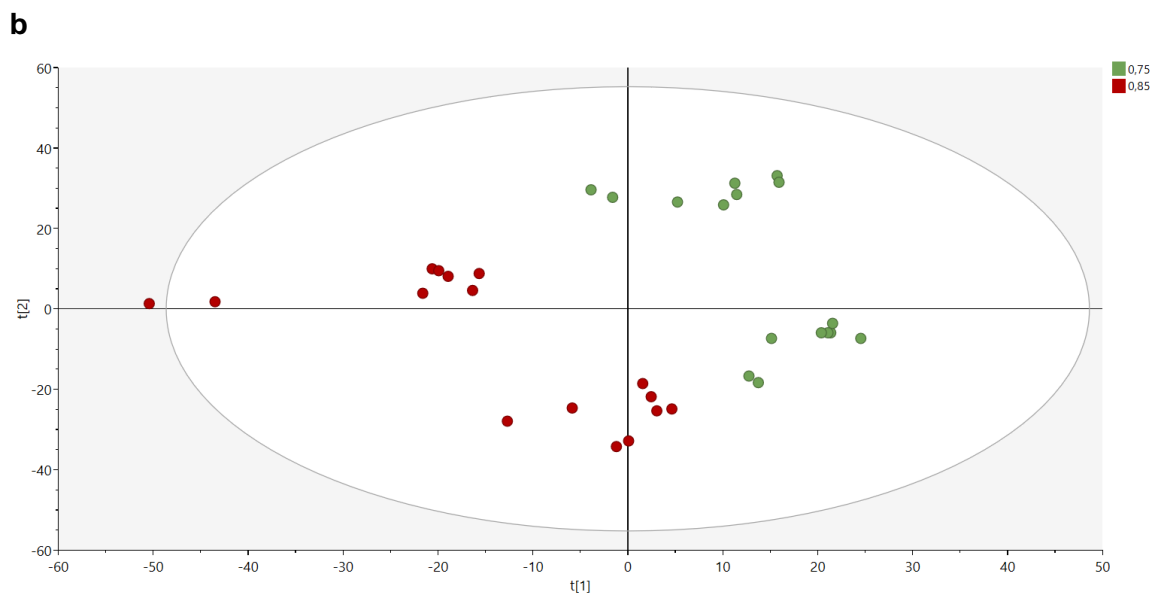
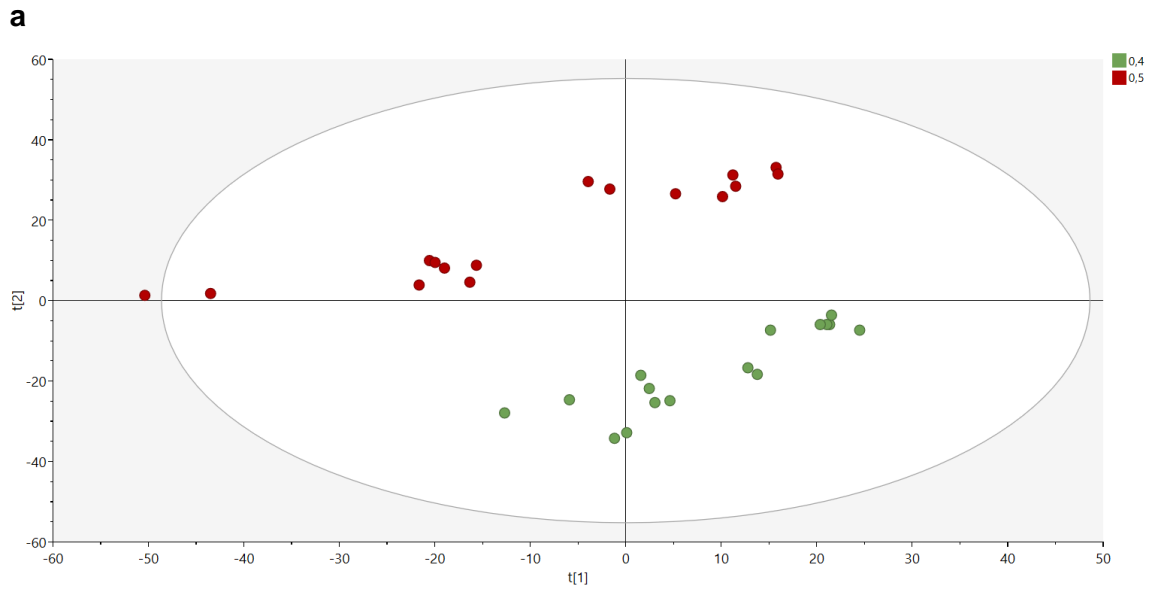


Figure 12 - Score plot for the z-factor tablet model. (a) Colored according to API content. Green: 40% API. Red: 50% API. (b) Colored according to SF level. Green: 0.75. Red: 0.85.

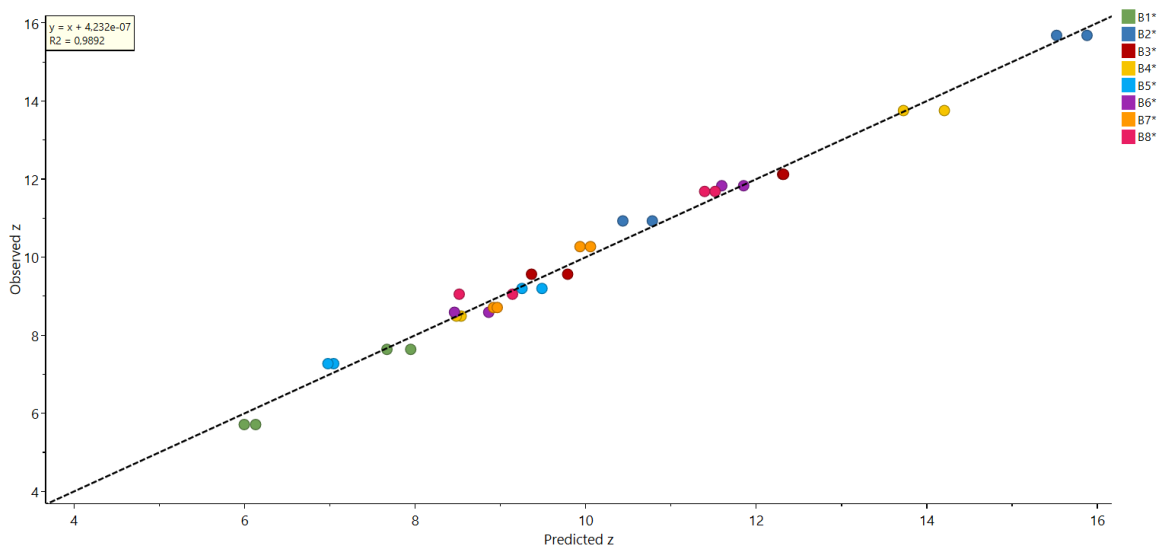


Figure 13 - Observed vs. Predicted regression line for the z-factor tablet model.

### 3.3.2 Erosion Model

#### Blends

Score plots of the erosion model were very similar to the z-factor model. Blends with different ibuprofen content seem to be more distributed along PC1, while PC2 separates blends with different lubricant content. This indicates that blend spectra might capture information on API and lubricant well and that such information has good correlation with the dissolution parameters.

Only slight differences are apparent in the distribution of scores. These differences are due to how each PLS model captures the relationships between the spectral data and the respective Y variables (the dissolution parameters). Different Y variables will cause the model to highlight different spectral regions and blend/tablet characteristics, leading to distinct score distributions, even when the underlying spectra are the same. To make this work less extensive, the plots can be consulted in annex A4.

The model was built using four components, with the following performance metrics (table 4):

- R<sup>2</sup>X: 0.63
- R<sup>2</sup>Y: 0.985
- Q<sup>2</sup>: 0.845

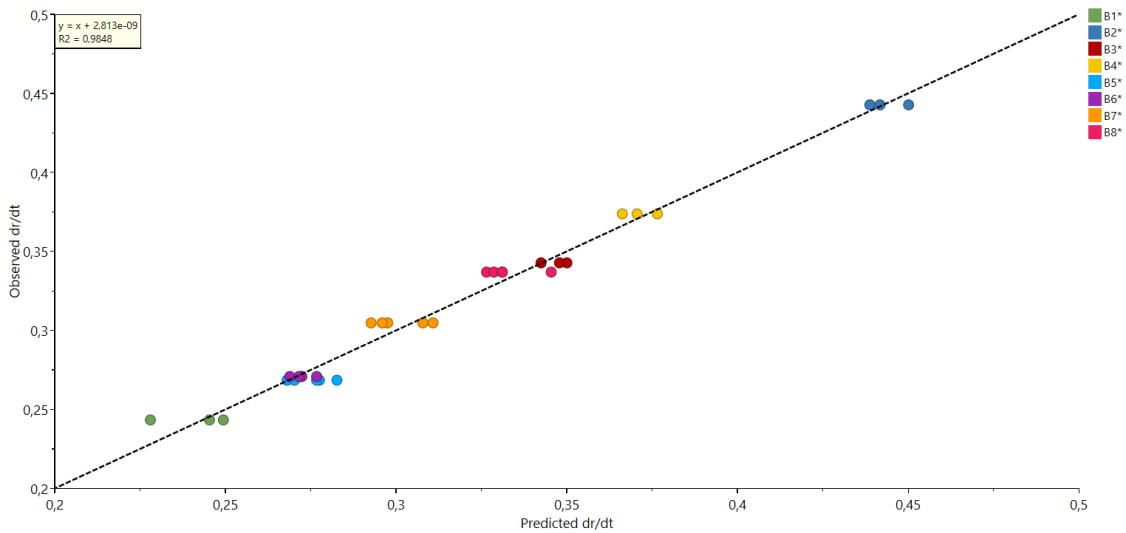


Figure 14 - Observed vs. Predicted regression line for the erosion blends model.

The regression line for observed versus predicted values of the parameter  $\frac{dr}{dt}$  for blends are shown in figure 14. As can be seen, data points are tightly clustered along the regression line.

### Tablets

Score plots of the erosion model for tablets can be consulted on annex A4. The scores distribution seems to vary more amongst tablet models than blend models. This could be because the process of compression introduces more variability in the spectra across different tablets.

Figure 15 shows the regression line of observed versus predicted values of  $\frac{dr}{dt}$  for tablets. Data points are tightly clustered along the regression line. The model was built using five components, with the following performance metrics (table 4):

R<sup>2</sup>X: 0.842

R<sup>2</sup>Y: 0.993

Q<sup>2</sup>: 0.917

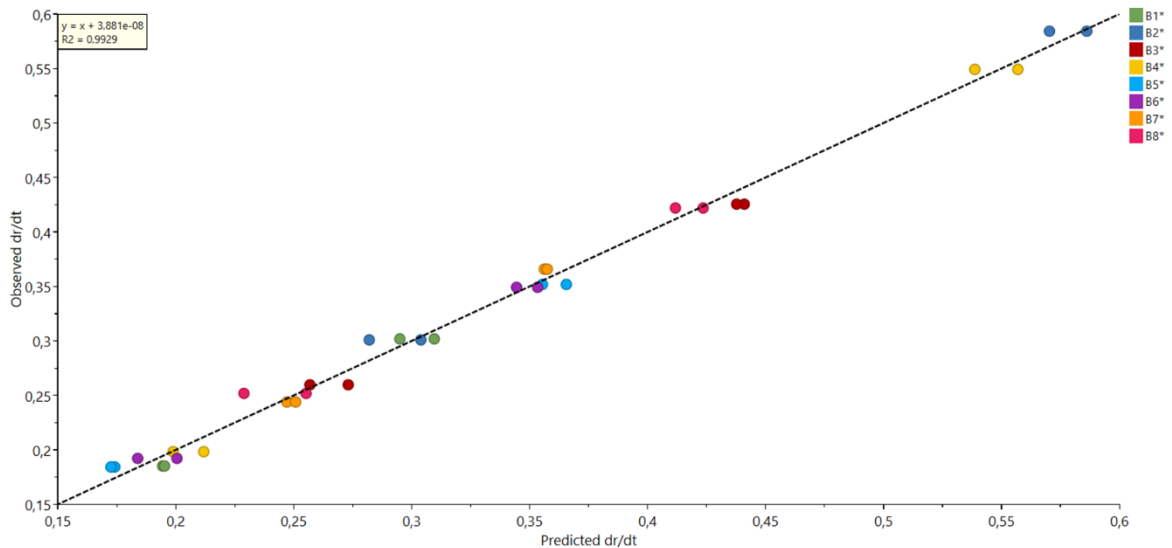


Figure 15 - Observed vs. Predicted regression line for the erosion tablet model.

### 3.3.3 Modified N-W Model

#### Blends

Score plots for the modified N-W model can be consulted in annex A5. The regression line for observed vs. predicted  $K$  values for the blends model is shown in figure 16. In this case, blend B5 appears to have the least precise predictions and overall, the data points are not as tightly clustered along the line. The model was built using four components, with the following performance metrics (table 3):

$R^2X$ : 0.626

$R^2Y$ : 0.975

$Q^2$ : 0.762

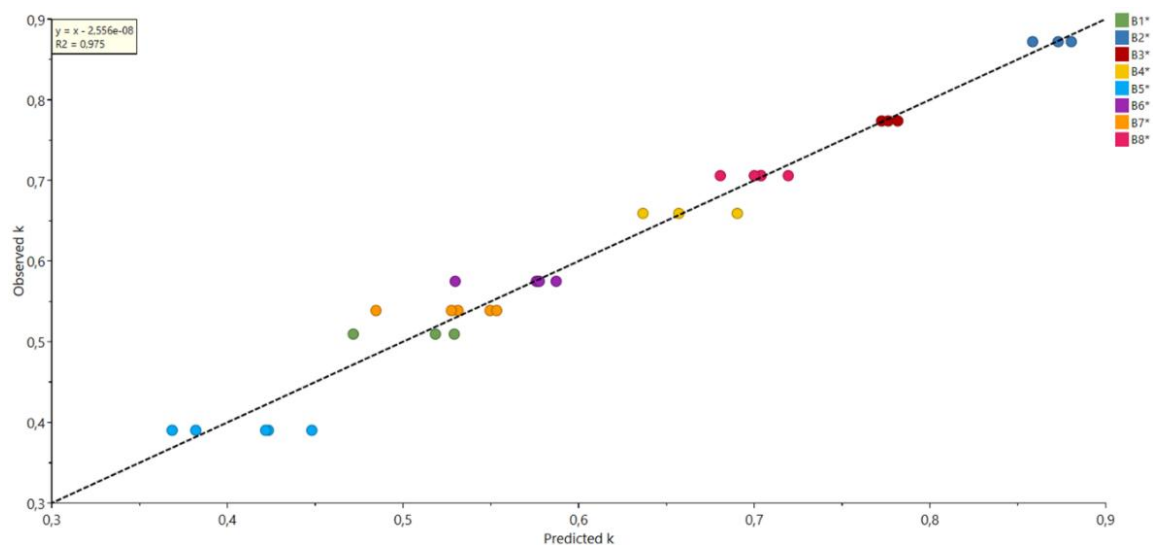


Figure 16 - Observed vs. Predicted regression line for the modified N-W blends model.

### **Tablets**

Figure 17 shows the regression line of observed versus predicted values of  $K$  for tablets. Data points are tightly clustered along the regression line. The model was built using five components, with the following performance metrics (table 3):

$R^2X$ : 0.84

$R^2Y$ : 0.993

$Q^2$ : 0.876

Scores plots for the modified N-W model are shown in annex A5.

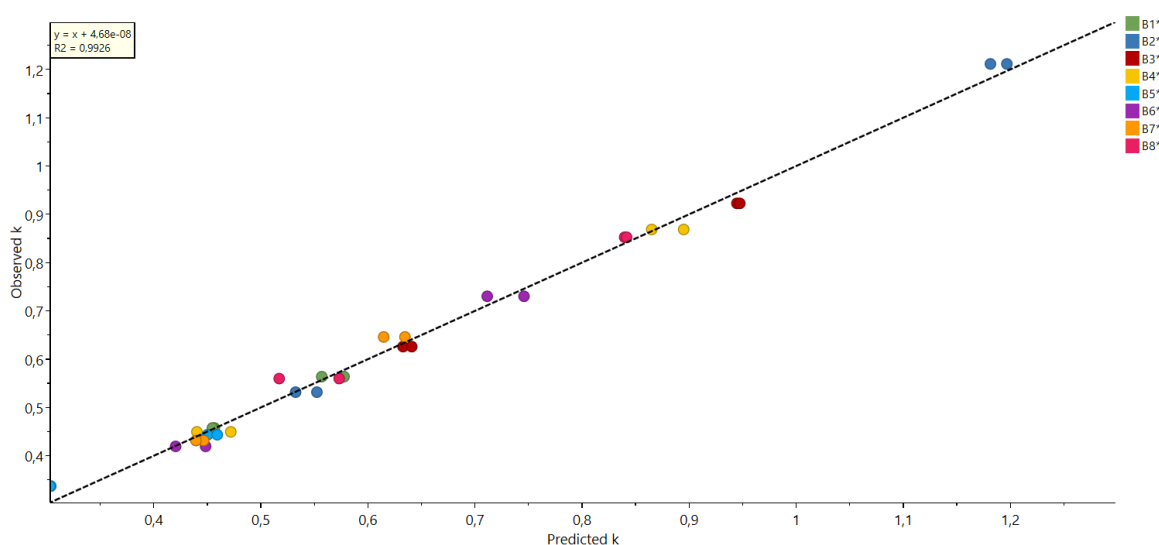


Figure 17 - Observed vs. Predicted regression line for the modified N-W tablets model.

### **3.3.4 Assay Prediction**

PLS models were also built to correlate spectral data with API content in order to evaluate the ability to predict the assay content in the blends and tablets. Figure 18a shows the observed vs. predicted API content in blends. For blends with 40% API content, predictions ranged from 38.5% to 41.5%, while blends with 50% API content showed predictions ranging from 48% to 51.5%.

Similarly, figure 18b depicts the observed vs. predicted API content in tablets. For tablets with 40% API content, predictions ranged from 39% to 41.5%, while tablets with 50% API content showed values between 48% and 52.5%. Two of the data points showed a higher prediction error but due to formatting issues with the plot, it is not possible to determine which specific tablets correspond to these points.

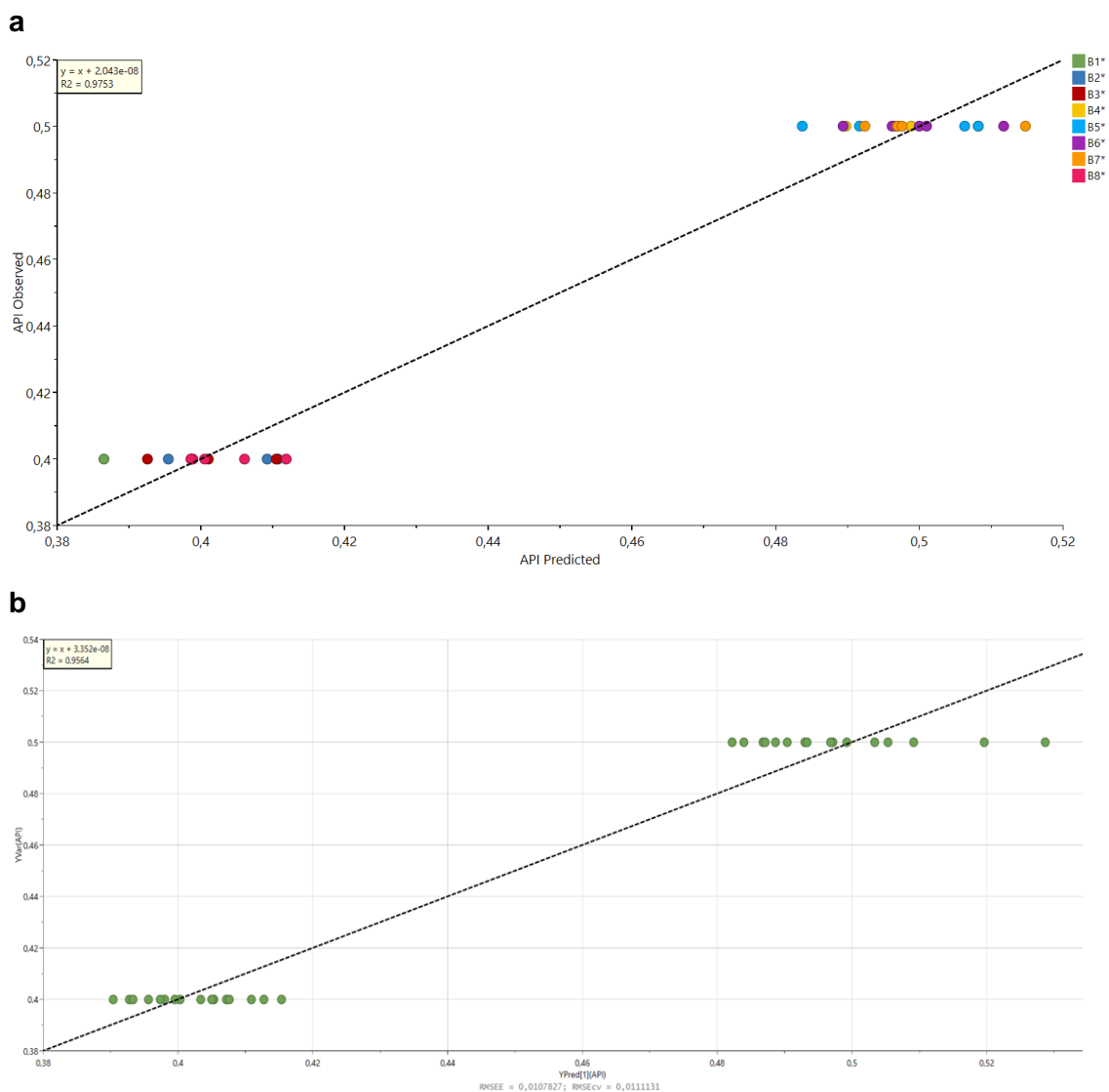


Figure 18 - Observed vs. Predicted regression line for the assay models of (a) blends, and (b) tablets.

These models were also used to predict the API content in the B9 blend and tablets, which have a different formulation than the calibration set (45% of ibuprofen). The mean API content predicted by the models was 41% for the B9 blend and 45% for the B9 tablet, meaning that the model that uses blend spectral data has less precise predictions.

### 3.4 Overview of Model Performance

To assess how well each equation fits the experimental data, the  $f_1$  (difference factor) and  $f_2$  (similarity factor) were calculated. These factors are typically used to compare the dissolution profiles of a reference product with a test product. In this case, they were used to compare experimental dissolution profiles with their corresponding modeled profiles.

The results, presented in table 3, indicate that all equations provide a good fit, with  $f_1 \leq 15$  and  $50 \leq f_2 \leq 100$ . Among the models, the modified Noyes-Whitney (N-W) equation demonstrates a slightly better fit, achieving the lowest  $f_1$  values and the highest  $f_2$  values. Both the erosion and z-factor models exhibit a similar performance.

Thus, regarding curve-fitting, the N-W model shows the best results, meaning the obtained equation parameters better represent the experimental data.

Table 3 - Calculated difference factor ( $f_1$ ) and similarity factor ( $f_2$ ) of the curve-fitted profiles.

Model	Mean $f_1$ (%)	Mean $f_2$ (%)
<b>z-Factor</b>	3.17 ± 1.06	71.87 ± 7.42
<b>Erosion</b>	2.98 ± 1.13	73.79 ± 7.95
<b>N-W</b>	2.09 ± 0.93	83.44 ± 6.80

Table 4 summarizes the performance metrics of the six models. The data indicates that models built using tablet data exhibit higher predictive power compared to those built with blend data.

It is worth noting that the  $R^2(X)$  in models built with blend data is significantly lower. The  $R^2(X)$  statistic evaluates how well the model captures the information of the independent variables. In this case, the components might not summarize well the variability in the X matrix because of the higher complexity and noise of blend spectral data. Also, blend data may have a less direct relationship to the equation parameters than tablet spectra, since the dissolution process is closely related to properties of the final tablet (e.g. the solid fraction level).

Despite all models presenting a high  $Q^2$ , it is the erosion tablet model that shows the highest value. The  $Q^2$  statistic is especially important, as it is a measure of the model's predictive ability. It indicates how well the models will predict new or unseen data.

For all models, the  $R^2(Y)$  values are consistently high, demonstrating a good fit to the training data. Among the models, the erosion model—of blends and tablets—shows the best performance across all evaluated parameters.

Table 4 - Performance metrics for all the models.

Model	Preprocessing	No. of components	R <sup>2</sup> (X)	R <sup>2</sup> (Y)	Q <sup>2</sup>
Blends	z-Factor	4	0.629	0.971	0.779
	Erosion	2 <sup>nd</sup> Derivative, SNV	4	0.630	0.985
	N-W		4	0.626	0.975
Tablets	z-Factor	5	0.838	0.989	0.825
	Erosion	SNV	5	0.842	0.993
	N-W	5	0.840	0.993	0.876

### 3.5 External Validation

External validation was carried out using the center point of the DoE (Batch B9, table 1, figure 2). This batch differs from the calibration data in both a different formulation and a SF level. Instead of curve-fitting, the rate parameters of each equation were predicted using the PLS models developed previously. The mean value for each model was used. Six spectra replicates were obtained from the blend, and two replicates were obtained from the tablet (front and back). Additionally, the mean predicted assay values for the B9 blend and tablet were included as input for predicted profiles. The confidence interval was calculated based on the RMSE<sub>c</sub>v given by SIMCA. Table 5 summarizes the predicted rate parameters for batch B9, along with the corresponding RMSE<sub>c</sub>v.

It is important to highlight that the real API content of batch B9 was 45% (180 mg). However, blend spectra used to build the PLS model may not have fully captured this information, leading to an underprediction. Table 5 provides all the predicted values obtained from the assay models.

Table 5 - Individual and mean rate parameters, and RMSE<sub>c</sub>v values obtained in SIMCA for blend and tablet models.

	Blends			Tablets		
	<i>z</i>	<i>dr/dt</i>	<i>K</i>	<i>z</i>	<i>dr/dt</i>	<i>K</i>
Individual	9.19	0.32	0.60	10.16	0.34	0.65
	9.06	0.31	0.62	11.61	0.41	0.75
	9.55	0.33	0.61	-----	-----	-----
	9.84	0.34	0.59	-----	-----	-----
	9.12	0.32	0.53	-----	-----	-----
	9.95	0.32	0.61	-----	-----	-----
Mean	<b>9.45</b>	<b>0.33</b>	<b>0.59</b>	<b>10.89</b>	<b>0.37</b>	<b>0.70</b>
RMSE <sub>c</sub> v	0.86	0.03	0.07	1.55	0.05	0.12

Table 6 - Assay content predicted for blend B9 and tablet B9, and respective mean values.

	Blends	Tablets
Individual (%)	37.9	45.3
	39.6	45.2
	40.4	-----
	41.8	-----
	41.7	-----
Mean (%)	42.7	-----
Mean (mg)	165.2	183.6

Figures 19, 20, and 21 compare the experimental dissolution profile of tablet B9 with the profiles predicted using the blend and tablet models.

Similar to the previous results, the dissolution of tablet B9 did not reach 100% (only 160 mg of API were released from the theoretical 180 mg of API content).

Since the z-factor and erosion models assume 100% release, it was necessary to adjust the dissolution profile according to equation 12. However, this adjustment was only performed to the dissolution profile compared with the z-factor and erosion models applied to the tablets. It was not necessary to apply if for the blend models, because coincidentally the assay from the blend was underpredicted (41% API content instead of the theoretical 45%).

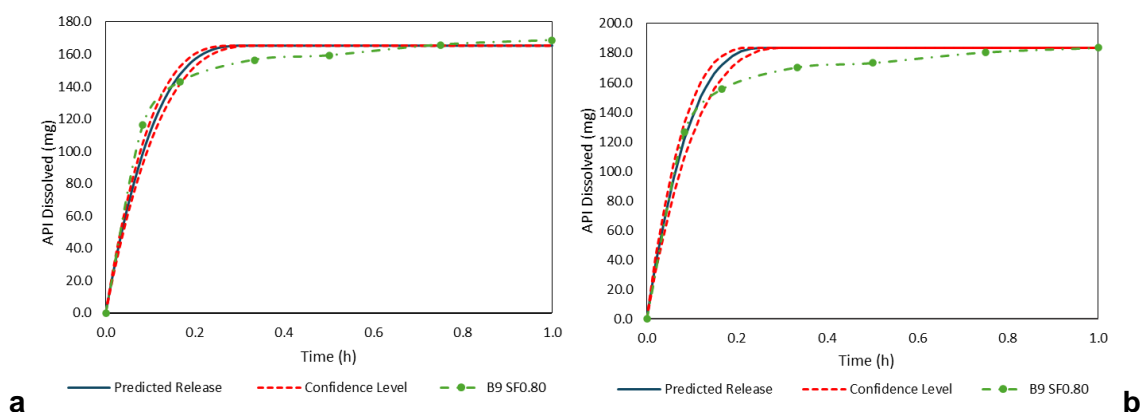


Figure 19 - External validation of the z-factor model. (a) Predicted from blend data. (b) Predicted from tablet data. Predicted dissolution profile (dark blue), confidence limits (red), experimental dissolution profile (green).

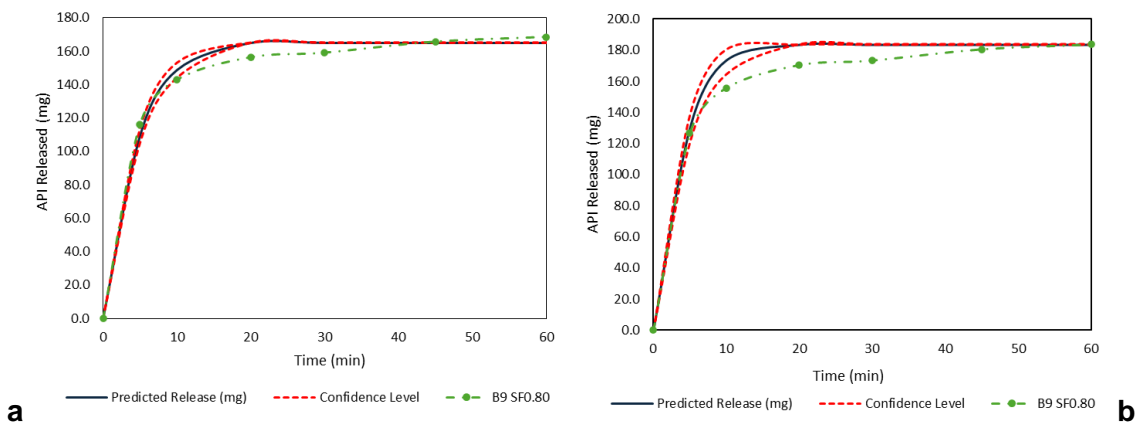


Figure 20 - External validation of the erosion model. (a) Predicted from blend data. (b) Predicted from tablet data. Predicted dissolution profile (dark blue), confidence limits (red), experimental dissolution profile (green).

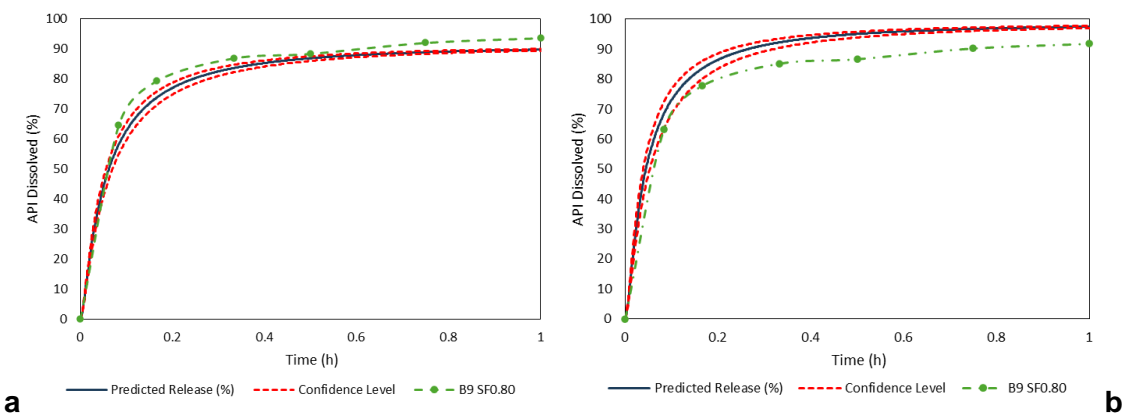


Figure 21 - External validation of the modified N-W model. (a) Predicted from blend data. (b) Predicted from tablet data. Predicted dissolution profile (dark blue), confidence limits (red), experimental dissolution profile (green).

To evaluate once again the fitting of each model to the experimental data,  $f_1$ ,  $f_2$ , and the RMSE of the profiles of batch B9 were calculated ( $RMSE_{diss}$ ). Additionally, the models were curve-fitted to the experimental dissolution profile to compare the fitted parameter with the model parameter predicted from the PLS model ( $RMSE_{par}$ ). The results are presented in table 7.

Table 7 - Calculated difference factor ( $f_1$ ), similarity factor ( $f_2$ ), and RMSE of the external validation.

Model	Blend				Tablet			
	$f_1$	$f_2$	$RMSE_{diss}$	$RMSE_{par}$	$f_1$	$f_2$	$RMSE_{diss}$	$RMSE_{par}$
z-factor	4.46	63.74	5.22	0.865	4.89	63.00	5.40	0.572
Erosion	3.46	71.69	3.54	0.026	4.16	67.09	4.44	0.074
Modified N-W	3.40	70.75	3.71	0.074	7.64	59.41	6.41	0.034

All of the profiles pass the criteria of  $f_1 \leq 15$  and  $f_2 \geq 50$ , demonstrating a good fit. Overall, the profiles predicted from blend data showed results closer to the mean  $f_1$  and  $f_2$  values, even if they fall outside the standard deviation range. The erosion and modified N-W (from blend) presented the best fit and had a very similar performance between them. The z-factor and erosion models showed fairly consistent results across blend and tablet data. Of all six models, the modified N-W profile predicted with tablet data showed the poorest fit. This can also be observed in figure 21b. However, it should be noticed that this might be due to the incomplete dissolution of the tablet, as the predicted profile is also based on the input of the predicted assay – about 45% of API content. Nonetheless, in the case of the tablet disintegration being significant, the modified N-W might be a better option as the approximate  $\frac{dr}{dt}$  was determined from the disintegration time.

The RMSE of the B9 parameters ( $RMSE_{par}$ ) predicted from blend models are in accordance with the  $RMSE_{cv}$ , which indicates there was no overfitting. For tablet models, the RMSE of the parameter was slightly lower than the  $RMSE_{cv}$ .

It is important to note that the external validation was performed with one sample only.

## 4 Final Considerations

While the results from the calibration of models and external validation are promising, they bring forward several questions.

Namely, the ability to accurately predict the assay content in blends/tablets is relevant, as this is a key input in all three equations tested. Inaccuracies in assay predictions compromise the reliability of the dissolution predictions. Thus, application of these dissolution models in an actual tableting line requires a validated model for assay prediction. NIR or Raman probes can be installed either in the feed frame of a compression machine (blend data) or tablet data can be acquired by an operator at-line. In this work, models using both blend and tablet spectral data were developed.

Equally important is the development of a robust dissolution method. For this work, none of the tablets tested achieved 100% of API dissolved. This was addressed by adjusting the dissolution data to the theoretical amount of API in the tablet, to avoid an offset between curve-fitted and experimental profiles. The third model, the modified N-W, does not require this adjustment as sink conditions are not assumed and so the API might not dissolve completely. Typically, however, this would not be a problem as 100% dissolution is a requirement.

A broader DoE, encompassing wider variations in formulation, should also be developed to calibrate the models. Additionally, different material lots and attributes, such as API particle size should also be considered. Regarding the impact of process parameters, only the compression force was evaluated, as tablets were produced with different solid fractions. This impact should be further assessed by varying furthermore the compression force. Other process parameters can also have an impact in the dissolution profile, such as blender speed, or paddle speed in the feed frame, which can promote over lubrication or impact the tablet attributes of strain sensitive formulations. Thus, product and process knowledge should also be acquired in order to understand which factors impact dissolution the most and to find the design space in which the dissolution profile remains within spec. In order to apply the dissolution model for real time release testing, the model must be able to predict the dissolution profile from batches within specification and also non-conforming batches.

Furthermore, external validation should be performed with a larger sample set and the MVAC must be defined.

Most of these points and requirements are further discussed in the FDA's article on RTRT-D. The article describes some expectations from regulatory entities regarding the development and application of dissolution models. For more information and insight, the reader is directed there.

## 5 Conclusions

In this thesis, a methodology for developing dissolution models at a laboratory scale was defined. Dissolution profiles were modelled by three different first-principles equations. Spectroscopic data was acquired from powder blends and directly compressed tablets and used to develop PLS models that correlated the spectral data to determined equation rate parameters. External validation with a small sample was performed. Regarding the calibration set, results from the PLS models showed good prediction capability and the results from the external validation agree with that. The dissolution profiles of batch B9 obtained with predicted parameters and assay content showed a good fit to the experimental data.

For a future work, suggestions include proper development of a dissolution method and an assay model, a more in-depth study of the process of tablet dissolution, a broader DoE, a larger sample set for external validation, and definition of the MVAC.

## References

1. Burcham, C. L., Florence, A. J. & Johnson, M. D. Continuous Manufacturing in Pharmaceutical Process Development and Manufacturing. (2018) doi:10.1146/annurev-chembioeng.
2. Deloitte Centre for Health Solutions. *Seize the Digital Momentum: Measuring the Return from Pharmaceutical Innovation 2022*. (2023).
3. Department of Health and Human Services & U.S Food and Drug Administration (FDA). *Pharmaceutical CGMPs for the 21st Century - A Risk-Based Approach (Final Report)*. (2004).
4. U.S Food and Drug Administration (FDA) & Department of Health and Human Services. PAT-A Framework for Innovative Pharmaceutical Development, Manufacturing and Quality Assurance. (2004).
5. Destro, F. & Barolo, M. A review on the modernization of pharmaceutical development and manufacturing – Trends, perspectives, and the role of mathematical modeling. *International Journal of Pharmaceutics* vol. 620 Preprint at <https://doi.org/10.1016/j.ijpharm.2022.121715> (2022).
6. Felder, R. M. & Rousseau, R. W. *Elementary Principles of Chemical Processes*. (John Wiley and Sons Inc, 2005).
7. Van Snick, B. *et al.* Continuous direct compression as manufacturing platform for sustained release tablets. *Int J Pharm* **519**, 390–407 (2017).
8. Schaber, S. D. *et al.* Economic analysis of integrated continuous and batch pharmaceutical manufacturing: A case study. *Industrial and Engineering Chemistry Research* vol. 50 10083–10092 Preprint at <https://doi.org/10.1021/ie2006752> (2011).
9. Goodwin, D. J., van den Ban, S., Denham, M. & Barylski, I. Real time release testing of tablet content and content uniformity. *Int J Pharm* **537**, 183–192 (2018).
10. European Medicines Agency. Guideline on Real Time Release Testing (formerly Guideline on Parametric Release). *EMA/CHMP/QWP/811210/2009-Rev1* **44**, 10 (2012).
11. International Conference on Harmonisation of Technical Requirements for Registration of Pharmaceuticals for Human Use. *ICH Harmonised Tripartite Guideline: Pharmaceutical Development Q8(R2)*. (2009).
12. International Conference on Harmonisation of Technical Requirements for Registration of Pharmaceuticals for Human Use. *ICH Quality Implementation Working Group: Points to Consider (R2)*. (2011).

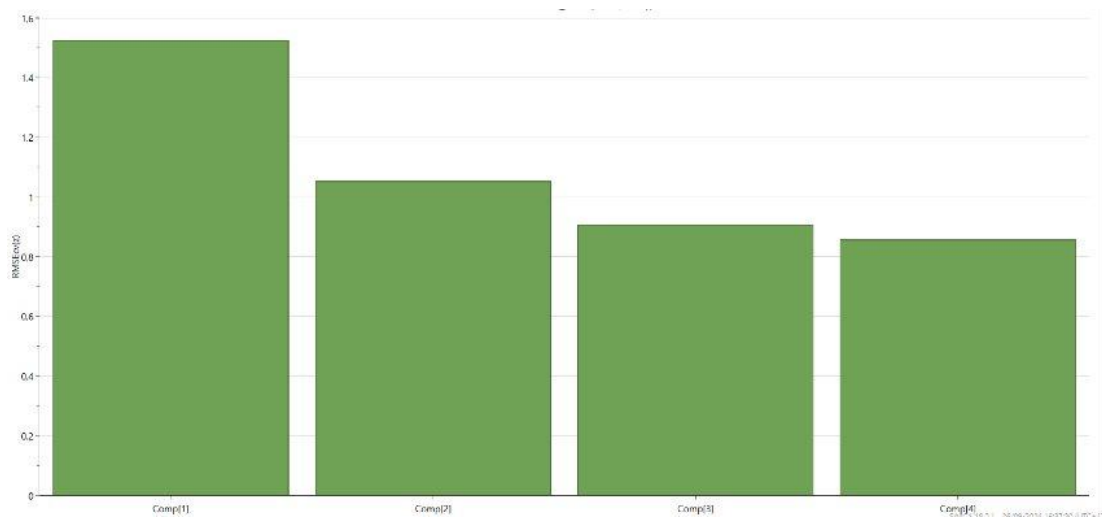
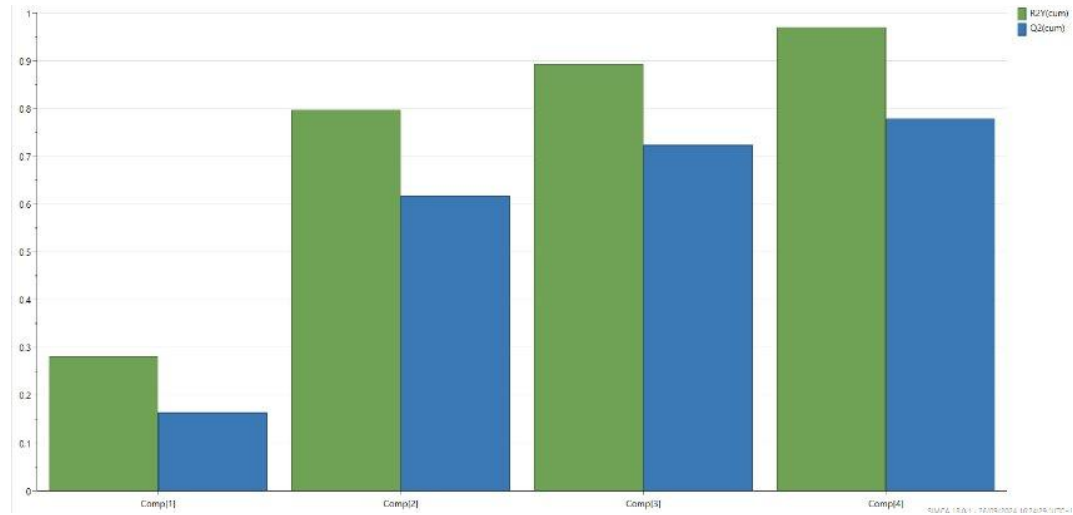
13. Kakhi, M., Li, J. & Dorantes, A. Regulatory Experience with Continuous Manufacturing and Real Time Release Testing for Dissolution in New Drug Applications. *J Pharm Sci* **112**, 2604–2614 (2023).
14. Jiang, M. *et al.* Opportunities and challenges of real-time release testing in biopharmaceutical manufacturing. *Biotechnol Bioeng* **114**, 2445–2456 (2017).
15. Markl, D. *et al.* Review of real-time release testing of pharmaceutical tablets: State-of-the art, challenges and future perspective. *Int J Pharm* **582**, (2020).
16. *Comprehensive Quality by Design for Pharmaceutical Product Development and Manufacture*. (Wiley, 2017).
17. Zaborenko, N. *et al.* First-Principles and Empirical Approaches to Predicting In Vitro Dissolution for Pharmaceutical Formulation and Process Development and for Product Release Testing. *AAPS Journal* **21**, (2019).
18. Zhao, Y., Li, W., Shi, Z., Drennen, J. K. & Anderson, C. A. Prediction of dissolution profiles from process parameters, formulation, and spectroscopic measurements. *J Pharm Sci* **108**, 2119–2127 (2019).
19. Noyes, A. A. & Whitney, W. R. The rate of solution of solid substances in their own solutions. *J Am Chem Soc* **19**, 930–934 (1897).
20. Florence, A. T. & Siepmann, J. *Modern Pharmaceutics - Volume 1. Modern Pharmaceutics* (Informa Healthcare USA, Inc., 2009).
21. Nicolaidis, E., Symillides, M., Dressman, J. B. & Reppas, C. *Biorelevant Dissolution Testing to Predict the Plasma Profile of Lipophilic Drugs After Oral Administration*. (2001).
22. Takano, R. *et al.* Oral absorption of poorly water-soluble drugs: Computer simulation of fraction absorbed in humans from a miniscale dissolution test. *Pharm Res* **23**, 1144–1156 (2006).
23. Hofsäss, M. A. & Dressman, J. Suitability of the z-Factor for Dissolution Simulation of Solid Oral Dosage Forms: Potential Pitfalls and Refinements. *J Pharm Sci* **109**, 2735–2745 (2020).
24. Kang, Y., Chen, J., Duan, Z. & Li, Z. Predicting Dissolution of Entecavir Using the Noyes Whitney Equation. *Dissolut Technol* **30**, 38–45 (2023).
25. Wilson, D., Wren, S. & Reynolds, G. Linking dissolution to disintegration in immediate release tablets using image analysis and a population balance modelling approach. *Pharm Res* **29**, 198–208 (2012).
26. Su, Q. *et al.* Model predictive in vitro dissolution testing in pharmaceutical continuous manufacturing: An equivalence study. *AIChE Journal* **69**, 1–12 (2023).

27. Hernandez, E. *et al.* Prediction of dissolution profiles by non-destructive near infrared spectroscopy in tablets subjected to different levels of strain. *J Pharm Biomed Anal* **117**, 568–576 (2016).
28. Pawar, P. *et al.* Enabling real time release testing by NIR prediction of dissolution of tablets made by continuous direct compression (CDC). *Int J Pharm* **512**, 96–107 (2016).
29. Freitas, M. P. *et al.* Prediction of drug dissolution profiles from tablets using NIR diffuse reflectance spectroscopy: A rapid and nondestructive method. *J Pharm Biomed Anal* **39**, 17–21 (2005).
30. Donoso, M. & Ghaly, E. S. Prediction of drug dissolution from tablets using near-infrared diffuse reflectance spectroscopy as a nondestructive method. *Pharm Dev Technol* **9**, 247–263 (2004).
31. Costa, P. & Lobo, J. M. S. Modeling and comparison of dissolution profiles. *European Journal of Pharmaceutical Sciences* **13**, 123–133 (2001).
32. Galata, D. L. *et al.* Real-time release testing of dissolution based on surrogate models developed by machine learning algorithms using NIR spectra, compression force and particle size distribution as input data. *Int J Pharm* **597**, (2021).
33. Wu, H., Lyon, R. C., Khan, M. A., Voytilla, R. J. & Drennen, J. K. Integration of Near-Infrared Spectroscopy and Mechanistic Modeling for Predicting Film-Coating and Dissolution of Modified Release Tablets. *Ind Eng Chem Res* **54**, 6012–6023 (2015).
34. Zaborenko, N. *et al.* Predictive Dissolution Models for Real-Time Release Testing: Development and Implementation – Workshop Summary Report. *Dissolut Technol* **29**, 150–172 (2022).

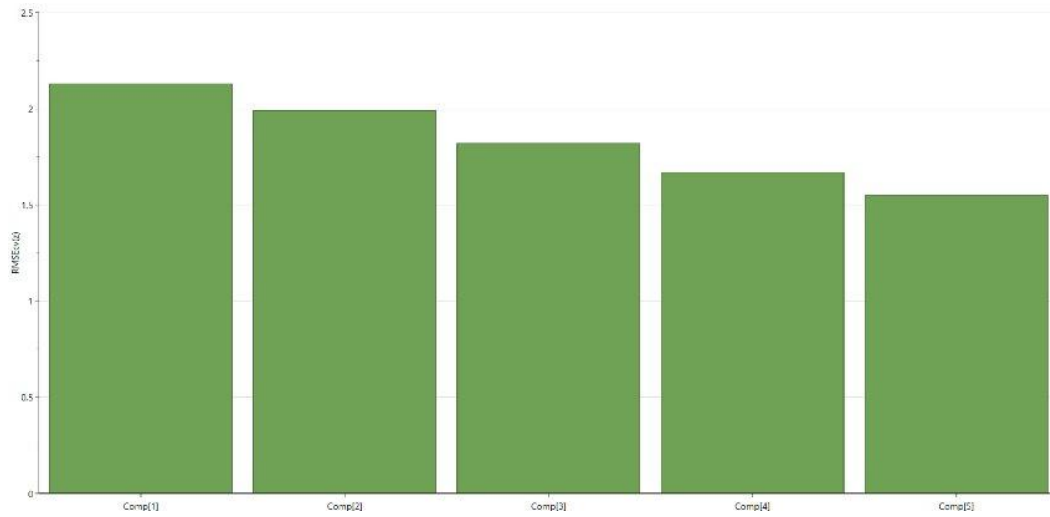
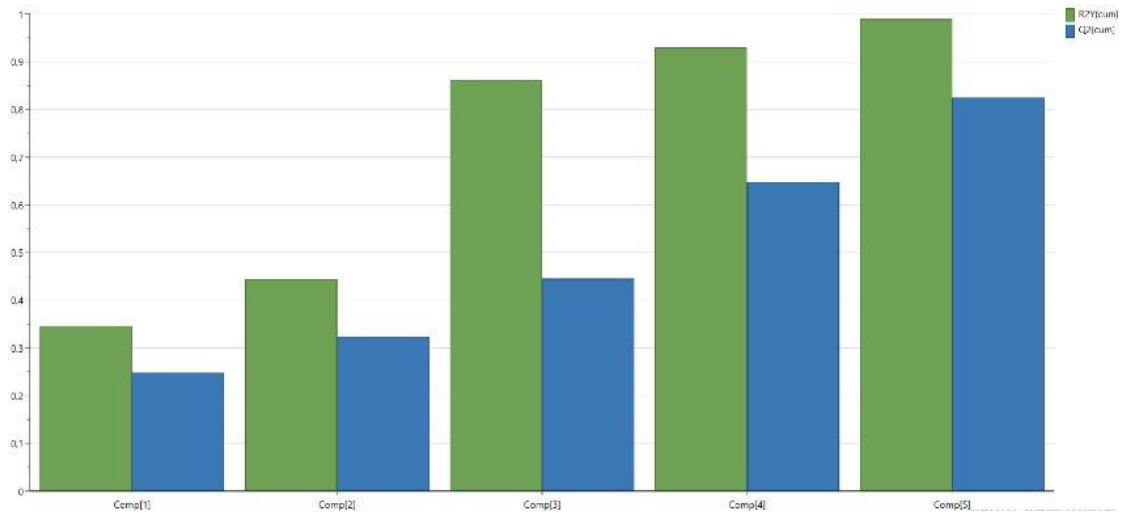
# Annexes

## A1. Summary of Fit and RMSECV – z-Factor

### Blends

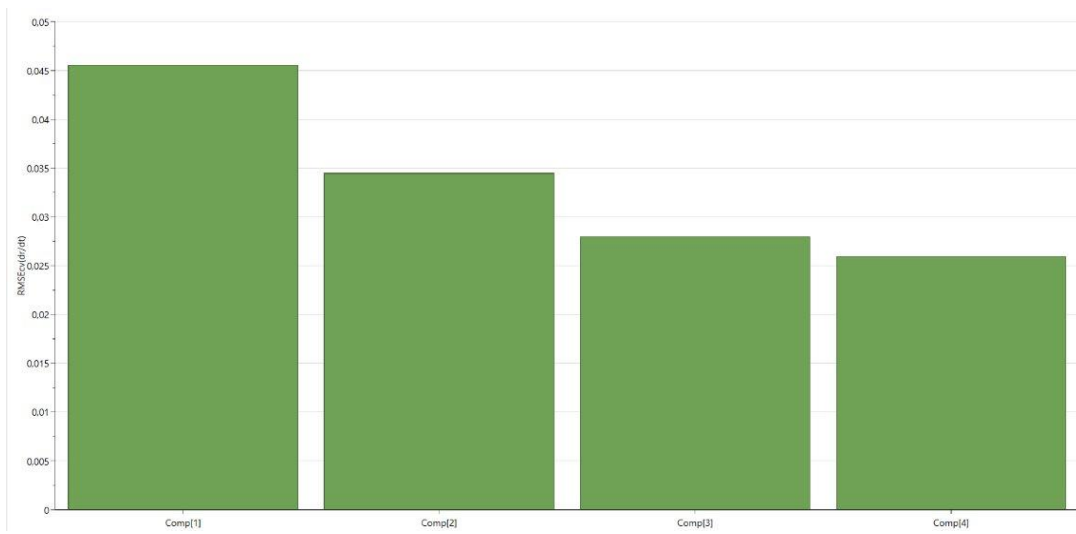
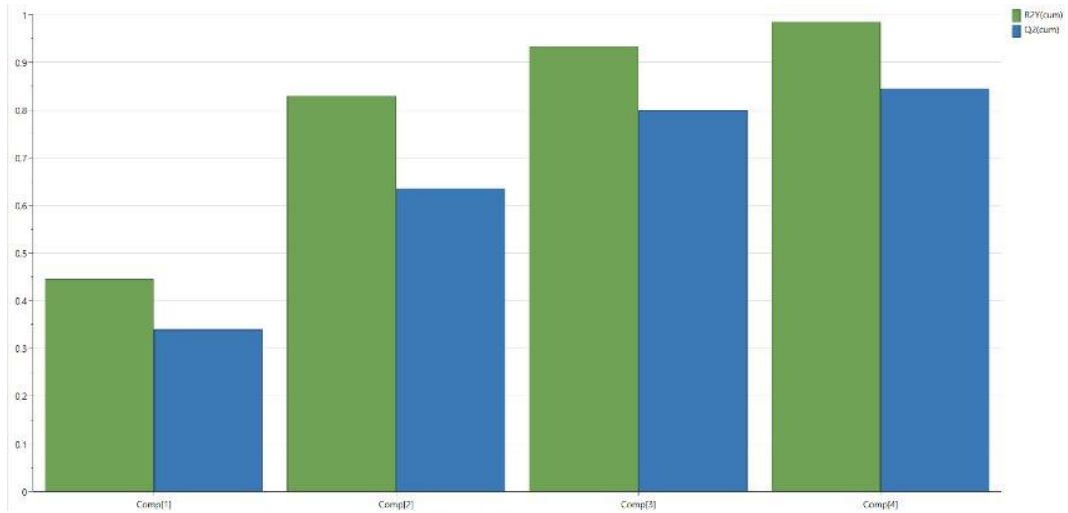


## Tablets

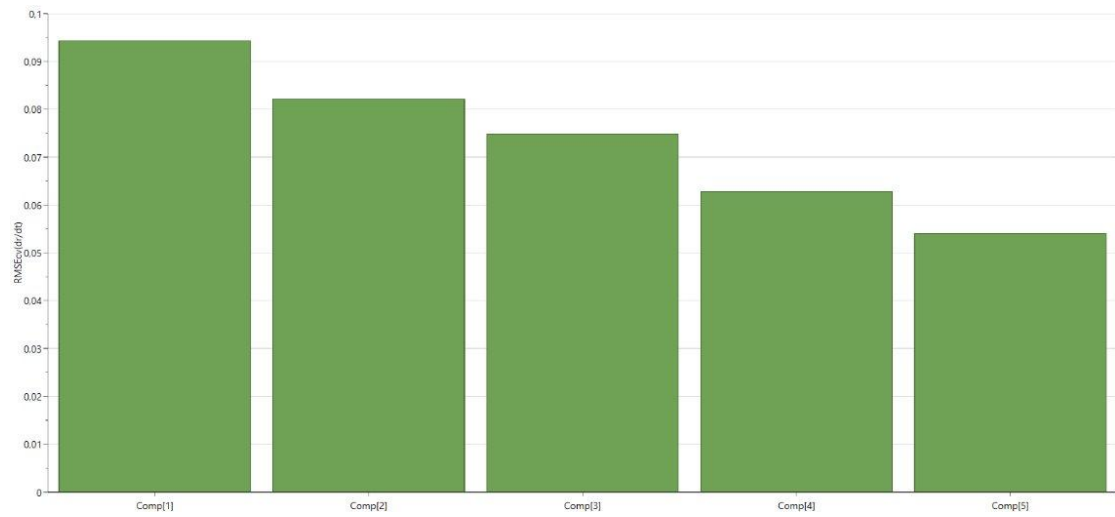
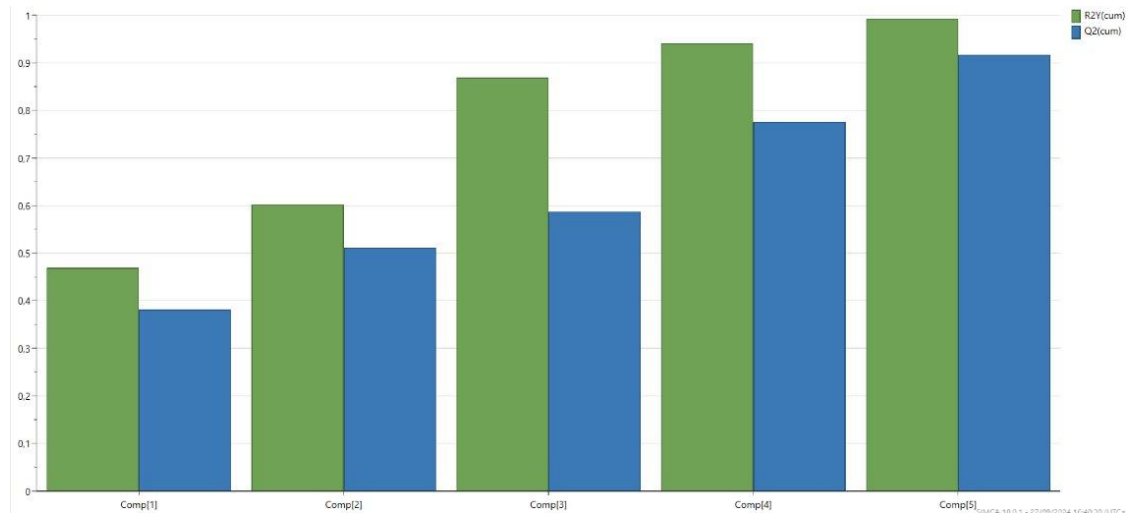


## A2. Summary of Fit and RMSECV – Erosion

### Blends

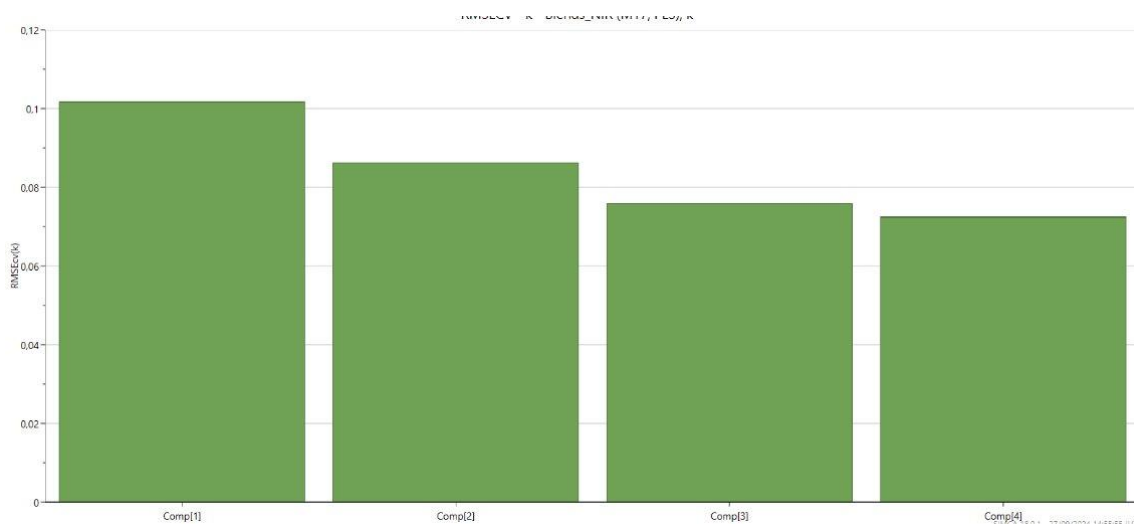
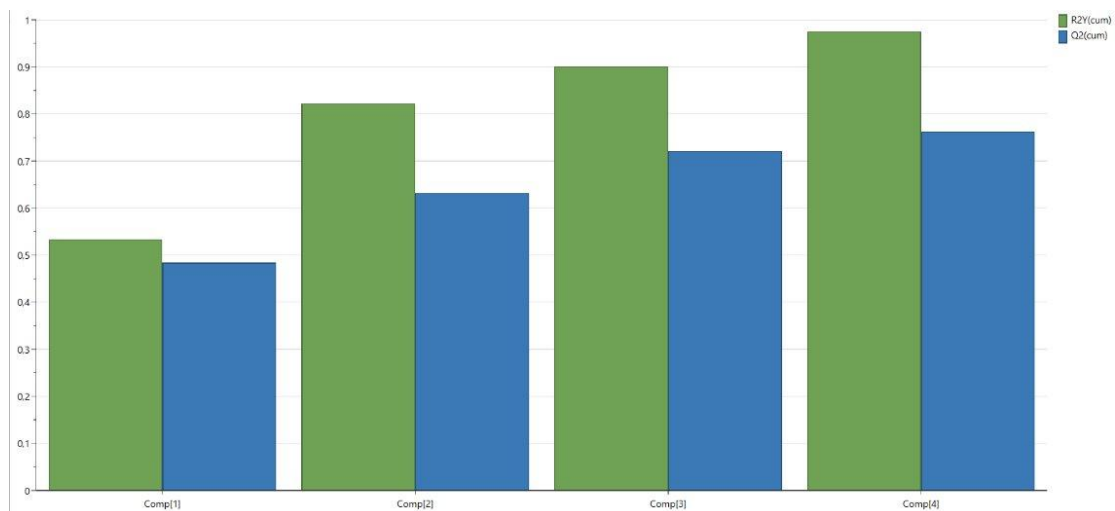


## Tablets

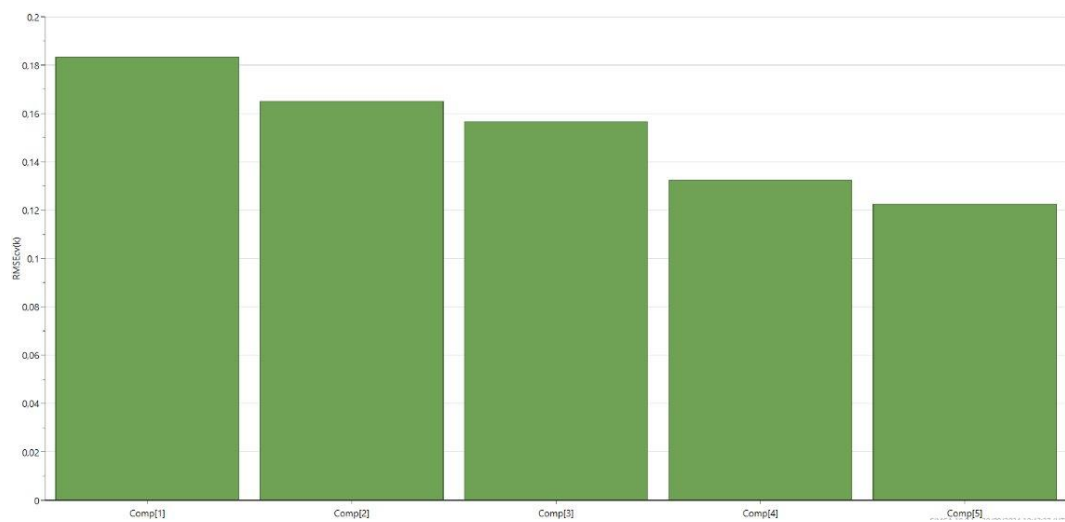
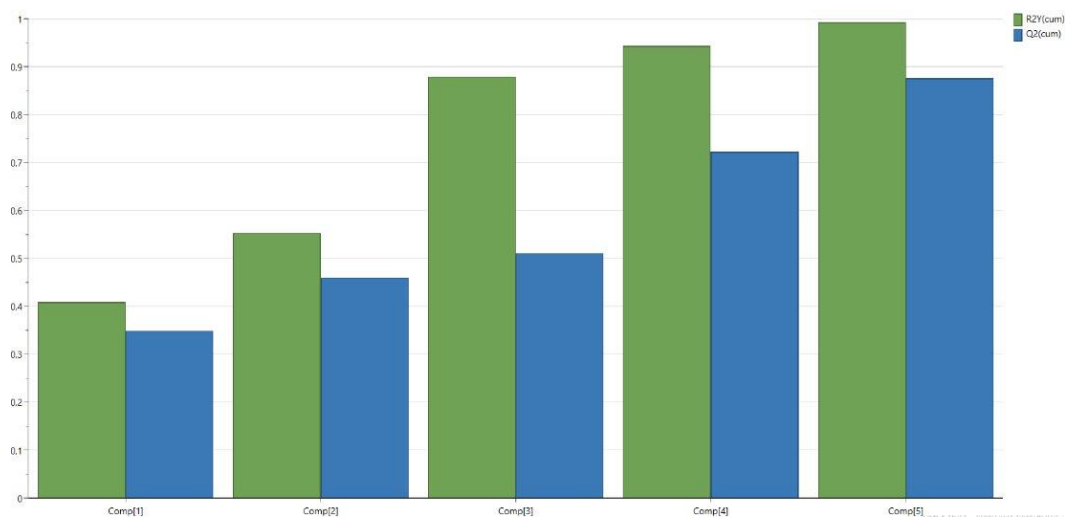


### A3. Summary of Fit and RMSECV – Modified N-W

#### Blends



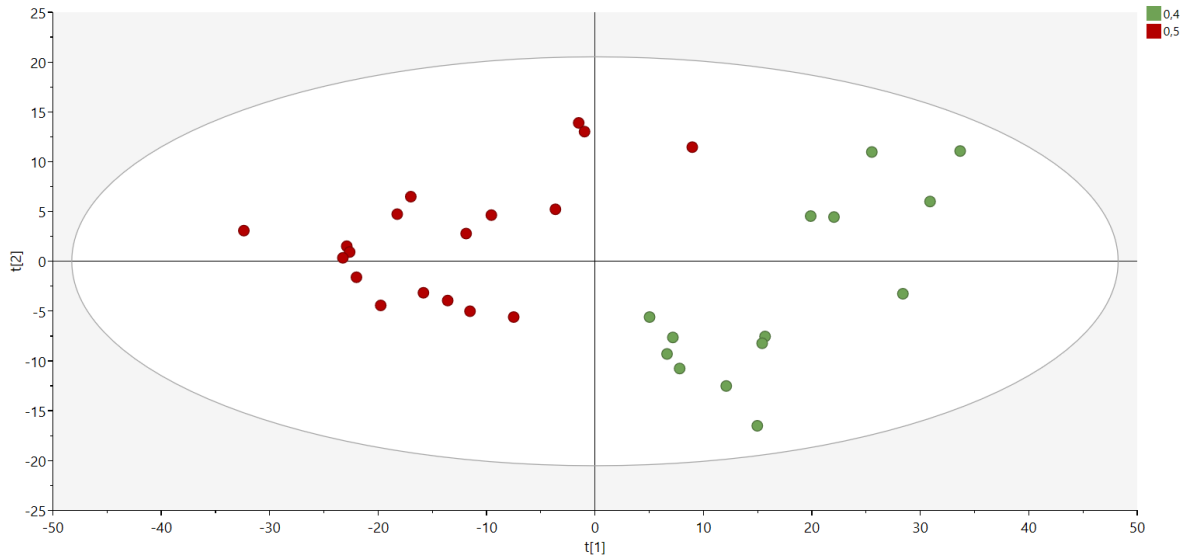
## Tablets



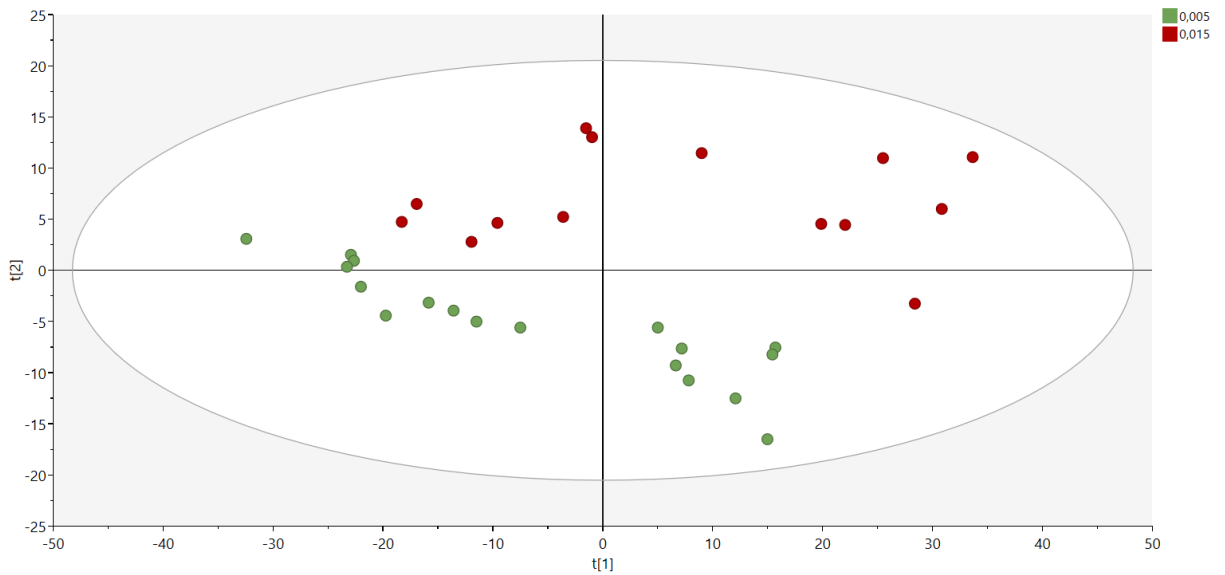
## A4. Score Plots (Erosion Model)

### Blends

Colored by API%

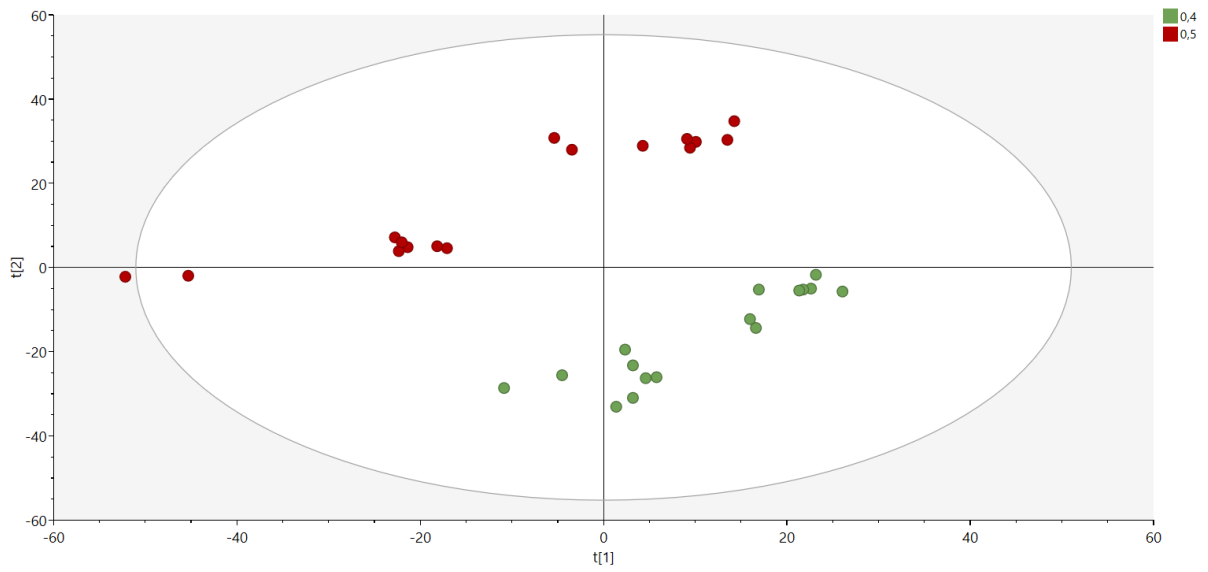


Colored by lubricant%

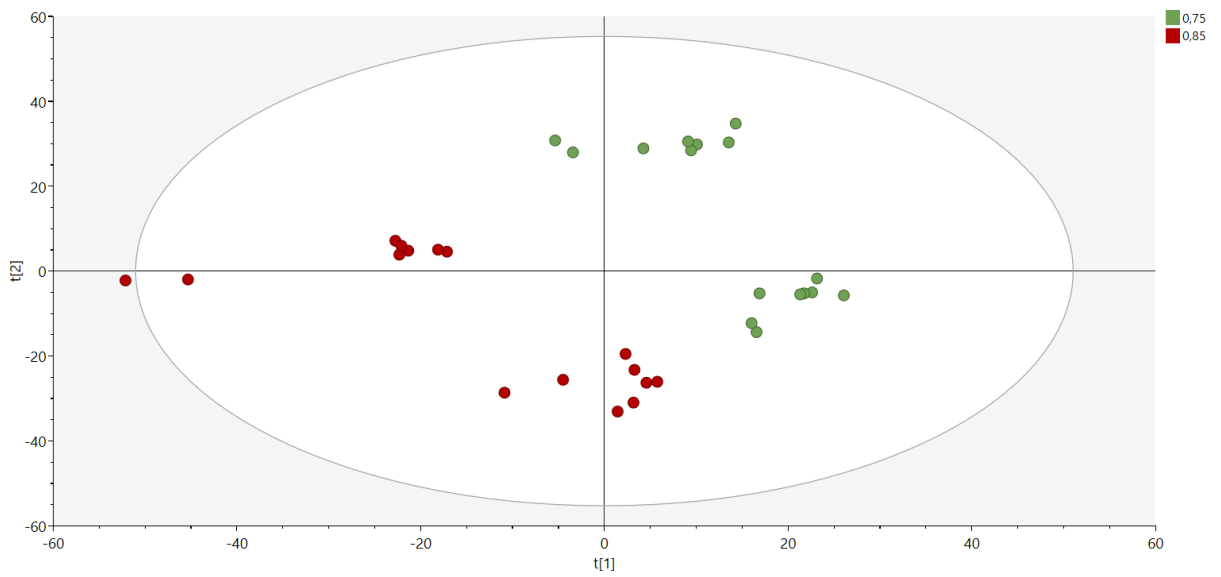


## Tablets

Colored by API%



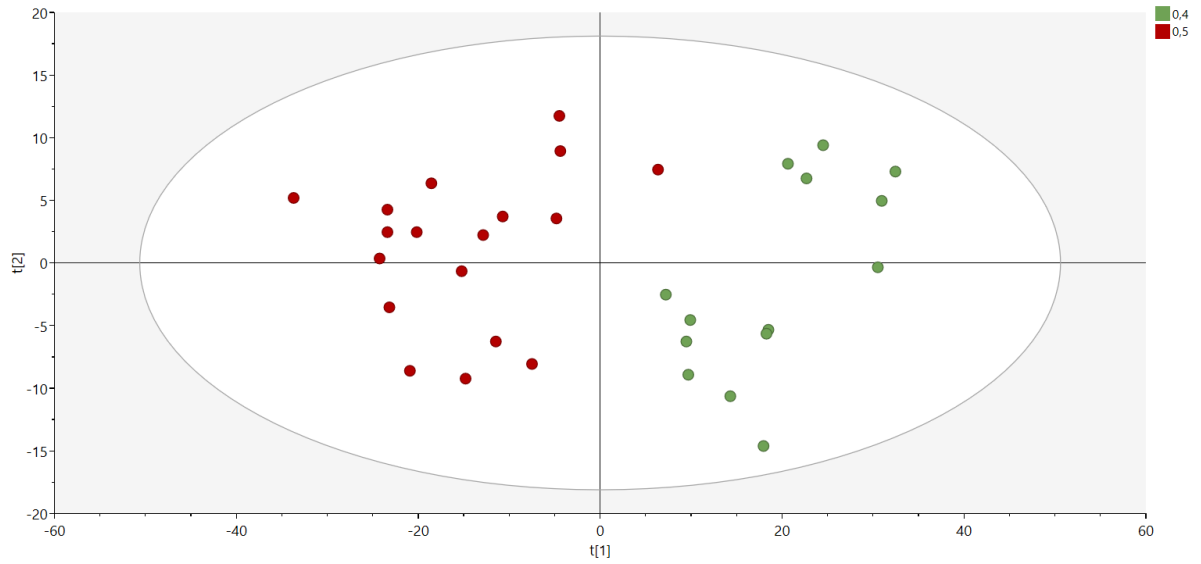
Colored by SF level



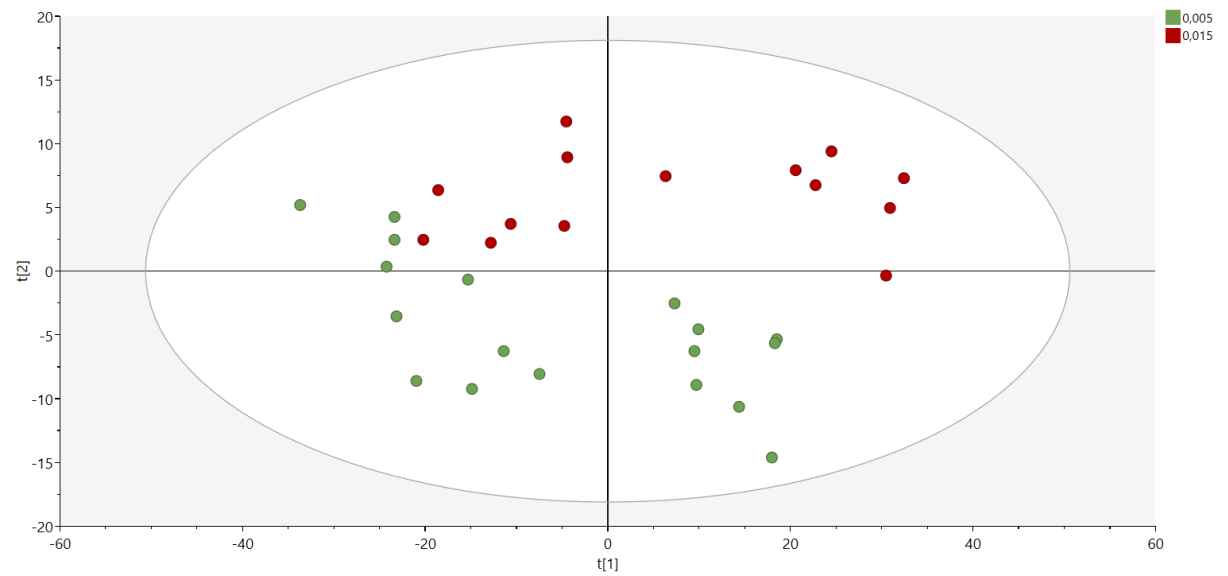
## A5. Score Plots (Modified N-W model)

### Blends

Colored by API%

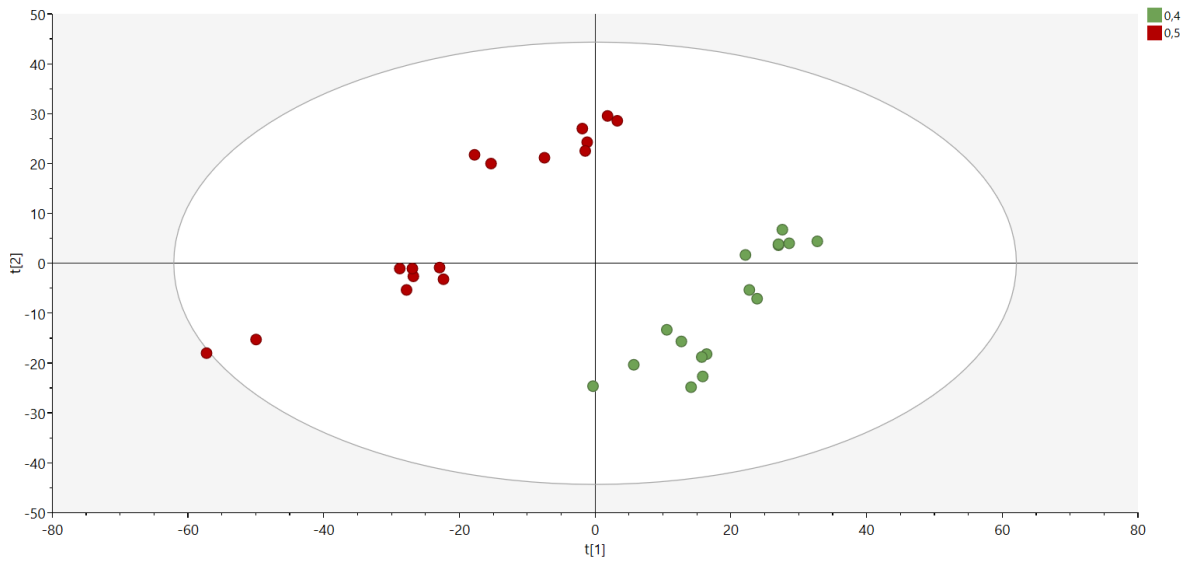


Colored by lubricant%



# Tablets

Colored by API%



Colored by SF level

